Epithelial-to-Mesenchymal Transition Supports Ovarian Carcinosarcoma Tumorigenesis and Confers Sensitivity to Microtubule Targeting with Eribulin

Gwo Yaw Ho[1,2,3], Elizabeth L. Kyran[1,2,4], Justin Bedo[1,5], Matthew J. Wakefield[1,6], Darren P. Ennis[7,8], Hasan B. Mirza[7], Cassandra J. Vandenberg[1,2], Elizabeth Lieschke[1,2], Andrew Farrell[1], Anthony Hadla[1,2], Ratana Lim[1], Genevieve Dall[1,2], James E. Vince[1,2], Ngee Kiat Chua[1], Olga Kondrashova[1], Rosanna Upstill-Goddard[8], Ulla-Maja Bailey[8], Suzanne Dowson[8], Patricia Roxburgh[8,9], Rosalind M. Glasspool[8,9], Gareth Bryson[10], Andrew V. Biankin[8]; for the Scottish Genomes Partnership, Susanna L. Cooke[8], Gayanie Ratnayake[3], Orla McNally[3,6,11], Nadia Traficante[11,12]; for the Australian Ovarian Cancer Study[12,13], Anna DeFazio[13,14,15], S. John Weroha[16], David D. Bowtell[11,12], Iain A. McNeish[7,8,9], Anthony T. Papenfuss[1,2,12], Clare L. Scott[1,2,3,6,11], and Holly E. Barker[1,2]

ABSTRACT

Ovarian carcinosarcoma (OCS) is an aggressive and rare tumor type with limited treatment options. OCS is hypothesized to develop via the combination theory, with a single progenitor resulting in carcinomatous and sarcomatous components, or alternatively via the conversion theory, with the sarcomatous component developing from the carcinomatous component through epithelial-to-mesenchymal transition (EMT). In this study, we analyzed DNA variants from isolated carcinoma and sarcoma components to show that OCS from 18 women is monoclonal. RNA sequencing indicated that the carcinoma components were more mesenchymal when compared with pure epithelial ovarian carcinomas, supporting the conversion theory and suggesting that EMT is important in the formation of these tumors. Preclinical OCS models were used to test the efficacy of microtubule-targeting drugs, including eribulin, which has previously been shown to reverse EMT characteristics in breast cancers and induce differentiation in sarcomas. Vinorelbine and eribulin more effectively inhibited OCS growth than standard-of-care platinum-based chemotherapy, and treatment with eribulin reduced mesenchymal characteristics and N-MYC expression in OCS patient-derived xenografts. Eribulin treatment resulted in an accumulation of intracellular cholesterol in OCS cells, which triggered a downregulation of the mevalonate pathway and prevented further cholesterol biosynthesis. Finally, eribulin increased expression of genes related to immune activation and increased the intratumoral accumulation of $CD8^+$ T cells, supporting exploration of immunotherapy combinations in the clinic. Together, these data indicate that EMT plays a key role in OCS tumorigenesis and support the conversion theory for OCS histogenesis. Targeting EMT using eribulin could help improve OCS patient outcomes.

Significance: Genomic analyses and preclinical models of ovarian carcinosarcoma support the conversion theory for disease development and indicate that microtubule inhibitors could be used to suppress EMT and stimulate antitumor immunity.

Introduction

Ovarian carcinosarcoma (OCS), also known as malignant mixed Müllerian tumor, is a heterogeneous cancer with poor prognosis (1), accounting for 1%-4% of ovarian malignancies (2, 3). These tumors contain both epithelial (carcinoma) and mesenchymal (sarcoma) components (3). Molecular analysis suggests that most OCS are monoclonal (4–9), with two theories for OCS histogenesis: combination, where a single stem cell differentiates early to form the two components; and conversion, where the carcinoma undergoes

[1]The Walter and Eliza Hall Institute of Medical Research, Parkville, Victoria, Australia. [2]Department of Medical Biology, University of Melbourne, Parkville, Victoria, Australia. [3]The Royal Women's Hospital, Parkville, Victoria, Australia. [4]Cancer Research UK Cambridge Institute, Cambridge, United Kingdom. [5]School of Computing and Information Systems, the University of Melbourne, Parkville, Victoria, Australia. [6]Department of Obstetrics and Gynaecology, University of Melbourne, Parkville, Victoria, Australia. [7]Division of Cancer and Ovarian Cancer Action Research Centre, Department of Surgery and Cancer, Imperial College London, London, United Kingdom. [8]Institute of Cancer Sciences, Wolfson Wohl Cancer Research Centre, University of Glasgow, Glasgow, United Kingdom. [9]Beatson West of Scotland Cancer Centre, Glasgow, United Kingdom. [10]Department of Pathology, Queen Elizabeth University Hospital, Glasgow, United Kingdom. [11]Sir Peter MacCallum Cancer Centre Department of Oncology, University of Melbourne, Parkville, Victoria, Australia. [12]Research Division, Peter MacCallum Cancer Centre, Melbourne, Victoria, Australia. [13]Centre for Cancer Research, The Westmead Institute for Medical Research, Sydney, Australia. [14]The Daffodil Centre, The University of Sydney, A Joint Venture with Cancer Council NSW, Sydney, Australia. [15]Department of Gynaecological Oncology, Westmead Hospital, Sydney, Australia. [16]Department of Oncology, Mayo Clinic, Rochester, Minnesota.

G.Y. Ho, E.L. Kyran, J. Bedo, and M.J. Wakefield contributed equally as co-authors of this article.

I.A. McNeish, A.T. Papenfuss, C.L. Scott, and H.E. Barker contributed equally as co-senior authors of this article.

Corresponding Author: Holly E. Barker, The Walter and Eliza Hall Institute of Cancer Research, 1G Royal Pde, Parkville, Victoria 3052, Australia. Phone: 613-9345-2350; Fax: 613-9345-0852; E-mail: barker.h@wehi.edu.au

Cancer Res 2022;82:4457–73

doi: 10.1158/0008-5472.CAN-21-4012

This open access article is distributed under the Creative Commons Attribution-NonCommercial-NoDerivatives 4.0 International (CC BY-NC-ND 4.0) license.

©2022 The Authors; Published by the American Association for Cancer Research

epithelial-to-mesenchymal transition (EMT) to form the sarcomatous component (10).

TP53 mutations and loss of heterozygosity (LOH) of 17p, and consequent chromosomal instability, are common in OCS (7, 8, 11, 12). Mutations in *PIK3CA*, *PTEN*, *KRAS*, *FBXW7*, *CTNNB1*, and *RB1* are observed frequently (11), whereas mutations in *ARID1A*, *ARID1B, KMT2D*, *BAZ1A*, *BRCA1*, *BRCA2*, and *RAD51C* have also been reported (8, 11, 13). One study also identified recurrent mutations in the genes encoding histones H2A and H2B (*HIST1H2AB/C* and *HIST1H2BB/G/J*) that play a role in EMT (9). Only one study has analyzed gene expression in the separate components, finding a strong positive correlation of EMT score with sarcoma content as well as methylation of the EMT-suppressing microRNAs *miR-141/200a/200b/200c/429* (8).

EMT can be induced through aberrant expression of the high-mobility group AT-hook protein 2 (HMGA2) and subsequent activation of the TGFβ signaling pathway (14). HMGA2 is not expressed in most adult tissues (15, 16), but high expression has been observed in many cancers and is correlated with metastasis and chemotherapy resistance (17–21). HMGA2 expression is thought to be largely controlled by the microRNA *let-7* (22). Other downstream target genes of *let-7* include *MYCN* and *LIN28B*, whereas LIN28B inhibits maturation of *let-7* (23), reinforcing both low and high expression states and acting as a bistable switch. Upregulation of the N-MYC/LIN28B pathway has been observed in the C5 subset of ovarian or fallopian tube high-grade serous carcinoma (HGSC) and in other cancer subtypes, and is associated with poor prognosis (23–25). Furthermore, high HMGA2 expression has been observed in 60% of OCS cases (26). We hypothesized that upregulation of the N-MYC/LIN28B pathway and subsequent expression of HMGA2 may be a key driver of OCS, and thus drugs that target EMT may be effective.

Eribulin is a microtubule-targeting drug that has been shown to reverse EMT, leading to favorable intratumoral vascular remodeling, reduced cell invasion, increased cell differentiation, and modulation of the tumor-immune microenvironment (27–29). Eribulin has completed Phase III trials for metastatic breast cancer, soft-tissue sarcoma and non–small cell lung cancer (NSCLC; refs. 30–33). Eribulin was initially approved by the FDA and the European Medicines Agency (EMA) in 2010 and 2011, respectively, for treatment of advanced breast cancer, with later approvals for advanced liposarcoma (28, 33). We hypothesized that eribulin may be effective against OCS tumors due to its ability to reverse EMT characteristics, alter tumor phenotype and affect the tumor microenvironment through effects on the vasculature.

Here we present mutation, copy number and gene expression analyses of separate components from an OCS cohort. We have used a highly relevant genetically engineered mouse model (GEMM), which replicates features of the human condition, as well as patient-derived xenograft (PDX) models of OCS to assess the efficacy of a range of microtubule-targeting drugs and to determine the mechanism of action of eribulin, a drug with significant activity in these models.

Materials and Methods

Study conduct, survival analyses, and patient samples

Samples for the UK cohort were acquired and used under the authority of the NHS Greater Glasgow and Clyde Biorepository (Application Reference 286) following approval by West of Scotland Research Ethics Committee 4 (Reference 10/S0704/60). Overall survival (OS) was calculated from the date of diagnosis to the date of death or the last known clinical assessment. OS was calculated by the log-rank test (Mantel–Cox) using Prism v8.0 (GraphPad).

Formalin-fixed paraffin-embedded (FFPE) specimens were identified from the pathology archives of Queen Elizabeth University Hospital, Glasgow, United Kingdom. Carcinoma and sarcoma regions were identified and marked by a gynecological pathologist.

Panel sequencing

Libraries for panel sequencing of isolated carcinoma and sarcoma regions of patient tumors were prepared from genomic DNA obtained from 5×10 μm macrodissected FFPE sections. Panel sequencing enabled analysis of 217 genes for coding sequence mutations, 137 genes for copy number state, and 23 genes for all genomic events. In addition, SNPs spaced approximately 1Mb apart throughout the genome were included to give a genome-wide copy-number profile. Full details of library preparation, panel design and sequencing analysis are provided in Supplementary Materials and Methods.

RNA preparation and sequencing

Libraries for RNA sequencing (RNA-seq) of isolated carcinoma and sarcoma regions of patient tumors were prepared from RNA obtained from 5×10 μm macrodissected FFPE sections. Libraries underwent 75bp paired-end sequencing on a HiSeq 4000 sequencer (Illumina). The HGSC samples from The Cancer Genome Atlas (TCGA; TCGA-OV cohort; $n = 396$) used for comparison were obtained from RNAseq_V2 processed counts downloaded from the GDC portal (https://portal.gdc.cancer.gov/), version available on June 3, 2019.

Libraries for RNA-seq of PDX tumors were prepared from RNA extracted using the Direct-zol RNA Miniprep kit (Zymo Research) as per manufacturer's instructions. Sequencing was performed on the Novaseq platform (Illumina) to read length of 100 bp (Australian Genome Research Facility). All analysis was performed on human specific reads, purified by competitive mapping of the reads to both the human and mouse genomes using our published opensource Xenomapper method (34). DEGs between treated and untreated samples were derived using matching methods across batch and model to correct for batch effects and inherent model differences. *P* values for DEGs were computed under a normality assumption. Topconfects (35) was used to calculate lower bounds on the effect sizes with 95% confidence interval. Full details of RNA-seq library preparation and sequencing analysis are provided in Supplementary Materials and Methods.

Generation of a GEMM

The *Pax8-rtTA* strain (C57BL/6 background) was a kind gift from Prof. Ronny Drapkin (Department of Obstetrics and Gynecology, University of Pennsylvania, Philadelphia, PA). The *kai-tetOCre* strain (FVB background) was a kind gift from Prof. Jane Visvader (WEHI, Melbourne, Australia) originally sourced from the Osaka Bioscience Institute, Japan. The *LSL-Lin28b* strain (mixed 129×1/SvJ background) was a kind gift from Prof. Johannes H. Schulte (University Hospital Essen, Essen, Germany). Full details about GEMM OCS tumor generation are available in Supplementary Materials and Methods.

Immunohistochemistry

Formalin fixed tumor samples were sectioned, stained with hematoxylin and eosin (H&E), or the following antibodies: anti-Ki67 (mouse: D3B5, Cell Signaling Technology; human: MIB-1, Dako), anti-PAX8 (Proteintech Cat# 10336–1-AP, RRID:AB_2236705), anti-p53 (mouse: CM5, Novacastra; human: DO-7, Dako), anti-PanCK (mouse: polyclonal, Abcam; human: AE1/3, Dako), anti-vimentin

(Cell Signaling Technology Cat# 5741, RRID:AB_10695459), anti-HMGA2 (Cell Signaling Technology Cat# 8179, RRID:AB_11178942), anti–N-cadherin (Abcam Cat# ab18203, RRID:AB_444317), anti-ZEB1 (Novus Cat# NBP1–05987, RRID:AB_2273178), anti-human CD8 (C8/144B, Dako). H&E and IHC slides were scanned digitally at ×20 magnifications using the Pannoramic 1000 scanner (3DHISTECH Ltd.). Ki67 and CD8 IHC were quantified using CellProfiler (Broad Institute).

Western blot analysis

Tumors and cells were homogenized in ice-cold RIPA buffer supplemented with a complete mini protease inhibitor cocktail tablet (Roche) using Precellys Ceramic Kit tubes in the Precellys 24 homogenizing instrument (Thermo Fisher Scientific). Proteins from lysates were separated on NuPAGE Novex Bis-Tris 10% gels (Invitrogen). Gels were transferred onto PVDF membranes using the iBlot Transfer system (Thermo Fisher Scientific). Membranes were probed with antibodies specific for ZEB1, N-cadherin, vimentin, HMGA2 (all as mentioned previously), N-MYC (Cell Signaling Technology Cat# 84406, RRID:AB_2800038), HMGCS (A-6, Santa Cruz Biotechnology), SQLE, LDLR (Proteintech Cat# 12544–1-AP, RRID:AB_2195888 and Proteintech Cat# 10785–1-AP, RRID:AB_2281164), Cleaved caspase-3 and cleaved PARP-1 (Cell Signaling Technology Cat# 9661, RRID:AB_2341188 and Cell Signaling Technology Cat# 5625, RRID:AB_10699459), or β-actin (Sigma-Aldrich Cat# A5441, RRID:AB_476744).

In vivo studies

All experiments involving animals were performed according to the animal ethics guidelines and were approved by the Walter and Eliza Hall Institute (WEHI) of Medical Research Animal Ethics Committee (2016.023). PDX #1040 was generated from ascites obtained from a patient treated at the Royal Women's Hospital, Melbourne, and recruited to the Australian Ovarian Cancer Study. The PDX was established by mixing tumor cells isolated from ascites with Matrigel Matrix (Corning) and transplanting subcutaneously into NOD/SCID/IL2Rγnull recipient mice (T1 = passage 1). PDX #1105 and #1177 were established through transplanting fragments of tumor tissue obtained from patients consented to the Stafford Fox Rare Cancer Program (WEHI, Melbourne, Australia). All other PDXs were established through transplanting fragments of cryopreserved tumor tissue subcutaneously from PDXs generated in the Mayo Clinic. Recipient mice bearing T2-T7 PDX or GEMM tumors (180–300 mm^3 in size) were randomly assigned to cisplatin (Pfizer), pegylated liposomal doxorubicin (PLD; Janssen-Cilag Pty. Ltd.), paclitaxel (Bristol–Myers Squibb), vinorelbine (Pfizer), eribulin (Eisai Co., Ltd.), or vehicle treatment groups. *In vivo* cisplatin treatments were performed by intraperitoneal (IP) injection of 4 mg/kg given on days 1, 8, and 18. The regimen for PLD treatment was by IP injection once a week for three weeks at 1.5 mg/kg. The regimen for paclitaxel treatment was by intraperitoneal injection twice a week for three weeks at 25 mg/kg. The regimen for vinorelbine was by intravenous injection of 15 mg/kg at days 1, 8, and 18. The regimen for eribulin treatment was by intraperitoneal injection three times a week for three weeks at 1.5 mg/kg (with the exception of mice harboring #1040 tumors, which received doses of 1 mg/kg with the same scheduling). Vehicle for cisplatin, PLD, paclitaxel, vinorelbine, and eribulin treatment was DPBS. Harvested tumors were histologically assessed by a gynecological pathologist, using sections stained with H&E, pan-cytokeratin and vimentin, to ensure both carcinoma and sarcoma components were present. See Supplementary Materials and Methods for dosing schedules and classification of treatment response. Data collection was conducted using the Studylog LIMS software (Studylog Systems). Graphing and statistical analysis was conducted using the SurvivalVolume package (36).

A human immune system (HIS) was generated in NSG mice by reconstituting myeloablated newborn NSG pups with human $CD34^+$ hematopoietic stem cells isolated from cord blood (purchased from Lonza, cat #2C-101). Briefly, 2-day old pups were treated with 150 rads gamma-irradiation and following 2–3 hours of recovery were injected via the facial vein with 5×10^4 human $CD34^+$ cells in 30–40 μL DPBS/0.02% trypan blue using a Hamilton syringe. Twelve-weeks post-reconstitution peripheral blood was obtained by retro-orbital bleed and analyzed using an Advia 2120i and, following red cell depletion, by flow cytometry (mCD45-APC/Cy7 clone 30-F11, hCD45-APC clone HI30, hCD4-BV605 clone RPA-T4, hCD8-FITC clone RPA-T8, hCD3-PE/Cy7 clone UCHT1, and hCD19-PE HIB19; BD Biosciences). Mice with >25% hCD45 white blood cells were considered successfully engrafted HIS mice. Tumor fragments for OCS PDX #1105 and #1177 were transplanted subcutaneously into HIS mice. Once tumors reached 400 mm^3, mice were treated with a single dose of vehicle (DPBS) or eribulin (3 mg/kg) and tumors were harvested one week later.

Generation of cell lines

The OCS GEMM cell line was generated from a T1 OCS GEMM tumor, the PH419 cell line was generated from a T3 PDX tumor, and the PH142 cell line was generated from a T5 PDX tumor. Briefly, tumors were manually minced into a slurry. For the GEMM cell line, cell fragments were subsequently plated on 0.1% gelatin coated plate and passaged aggressively within 3–4 days to retain viable malignant adherent cells until a stable cell line was obtained at passage 12 onward. For the PH419 and PH142 cell lines, the mince was digested with collagenase, dispase, and DNase (Worthington), with cells cultured in growth media for 10 passages. Cell identity was confirmed by genotyping (GEMM cell line) or *TP53* sequencing (PH419 and PH142 cell lines). Short tandem repeat profiling has also been used to characterize these new OCS cell lines.

Adhesion, invasion assays, and 3D growth assays

Adhesion assays were carried out in 96-well plates precoated with 2% BSA or 20 μg/mL collagen. GEMM cells were pretreated for a week with DMSO (vehicle control), 0.2 μmol/L cisplatin or 20 nmol/L eribulin (IC_{20} concentrations for these drugs in these cells) before plating in 96-well plates. Non-adherent cells were aspirated and adherent cells stained with 100 μL of 0.5% crystal violet (Sigma) dissolved in 20% methanol for 15 minutes at room temperature. Stained cells were solubilized with 50 μL of 0.1 mol/L citrate buffer in 50% methanol. Adherent cells were quantified by measuring absorbance at 595 nm on a Chameleon Luminescence Plate Reader (Noki Technologies). Transwell migration, invasion and 3D assays were carried out as previously described (37).

Quantification of cholesterol

Snap-frozen cell pellets or tumor pieces were lysed in 1X reaction buffer on ice. Cholesterol was quantified using the Amplex Red Cholesterol Assay Kit (Invitrogen) as per the manufacturer's instructions. Total cholesterol levels were quantified using buffer containing cholesterol esterase. Free cholesterol levels were quantified using buffer without cholesterol esterase. Cholesterol ester levels were calculated by subtracting the value of free cholesterol from total cholesterol.

Oil Red O staining

Snap-frozen tumor pieces were set in Optimal Cutting Temperature compound on dry ice and sectioned onto charged slides. Slides were incubated in Oil Red O solution, washed and counterstained with hematoxylin. Slides were scanned digitally at ×20 magnifications using the Pannoramic 1000 scanner (3DHISTECH Ltd.). Oil Red O staining was quantified using CellProfiler (Broad Institute).

Statistical analysis

Data were analyzed using the Student *t* test unless otherwise stated and considered significant when the *P* value was of <0.05. All statistical tests were two-sided. Bar graphs represent the mean and SE across independent experimental repeats (at least $n = 3$) unless otherwise stated. All boxplots demarkate the inter-quartile range as the outer box and median as the contained break. Whiskers extend to the furthest point not exceeding 1.5 × IQR. Survival analysis was performed using the log rank test on Kaplan–Meier survival function estimates. Statistical significance representations: *, $P < 0.05$; **, $P < 0.01$; ***, $P < 0.001$; and ***, $P < 0.0001$.

Data availability

The following datasets have been deposited in the European Genome-Phenome Archive (EGA) under accession number EGAS00001006555: RNA-seq data of the PDX samples, and TSO500 panel data, whole-exome sequencing (WES) data, or whole-genome sequencing data of the patient samples: PH003, PH006, PH142, PH419, PH592, #1105, and #1177. A data transfer agreement is required. The following datasets have been deposited in the EGA under accession number EGAS00001006605: DNA and RNA sequencing data of patient samples in the UK cohort ($n = 18$).

Results

Mutation and copy-number profile of OCS is similar to HGSC

We identified 18 women diagnosed with OCS, 17 with HGSC, and one with grade 2 endometrioid histology in the carcinoma component. 12 associated metastatic samples were also available (Supplementary Table S1 and Supplementary Fig. S1). As has previously been observed in uterine carcinosarcoma (38), the metastases in our cohort were more commonly purely carcinoma (8 carcinoma vs. 4 sarcoma; **Fig. 1A**; Supplementary Table S1).

Targeted sequencing of 377 genes in macrodissected carcinoma and sarcoma components as well as metastases was performed (Supplementary Tables S2–S7; Supplementary Fig. S2). Overall, OCS samples had genomic profiles similar to HGSC, with near-ubiquitous *TP53* mutation (17/18 cases, including 17/17 with HGSC pathology), *CCNE1* amplification (4/18 cases), *BRCA2* loss or mutation (4/18 cases), *KRAS* mutation and amplification (4/18 cases), *PIK3CA* mutation and amplification (4/18 cases), *NF1* or *CDKN2A* mutation or disruption by rearrangement (2/18 cases each), *RB1* deletion (2/18 cases), *PTEN* mutation (2/18 cases), and *MYC* or *MYCN* amplification (1/18 and 2/18 cases, respectively; **Fig. 1A**). Overall mutational burden was low (mean 1.2, median 0.87 mutations/MB sequenced), which did not differ between carcinoma and sarcoma (**Fig. 1B**; Supplementary Table S8). However, as with HGSC, the genomes were structurally unstable with an average of 3.3 high-level gains and 1.4 likely homozygous deletions called per sample (Supplementary Fig. S3). WW00163 lacked the genomic chaos typical of HGSC (Supplementary Fig. S4) in keeping with an origin of endometrioid carcinoma.

On the basis of the point mutation profiles, there were no consistent differences between the sarcoma and carcinoma components. In all cases, the two components shared at least one point mutation, demonstrating a shared clonal origin. Half of carcinoma–sarcoma pairs (8/16) shared all point mutations whereas the others gained additional mutation(s) in one or both components. On average, carcinoma–sarcoma pairs differed by only a single mutation (range, 0–7). These data indicated that these 18 OCS were monoclonal, which supports both the conversion and combination theories of carcinogenesis.

By contrast, there were more copy-number changes between the carcinoma and sarcoma components, with an average of 10.6 genes having a different copy-number state between the two (range, 0–36; Supplementary Figs. S3 and S4; Supplementary Table S6). The most commonly different genes were *FGF3* and *MDM2* (Supplementary Table S7). However, these differences did not appear to be focal or high level, perhaps suggesting that these genes are not specific targets of alteration between carcinomas and sarcomas. Instead these chromosomal differences may arise due to ongoing chromosomal instability. Case WW00169 had neither mutation nor copy-number differences between the carcinoma and sarcoma components.

Interestingly, in some cases metastases showed substantial genomic divergence from their corresponding primary, indicative of an early seeding to the metastatic sites (**Fig. 1A**). There was evidence of the metastases arising from the carcinomatous component (WW00158 and WW00170) as well as the sarcomatous component (WW00157). In addition to two cases (WW00154, WW00158) where the metastasis either gained three mutations or lost four, a third case (WW00157) diverged in several likely driver copy-number events, including loss of *BRCA2* between the carcinoma and its corresponding metastasis (Supplementary Tables S4, S6, and S7).

OCS have EMT-like and N-MYC pathway gene expression patterns

We next undertook RNA-seq on isolated carcinoma ($n = 13$) and sarcoma ($n = 9$, 7 paired with carcinoma) components (Supplementary Fig. S5; Supplementary Tables S9–S12). Using an EMT expression signature derived from uterine carcinosarcoma (39), we found a highly significant enrichment of EMT in carcinosarcomas, compared with the TCGA cohort of ovarian HGSC (TCGA-OV; $n = 379$). This enrichment was predominantly driven by the sarcoma component, with the EMT score being significantly higher in the sarcoma component compared with the carcinoma component ($P = 0.005$; **Fig. 1C**), and was confirmed using other reported EMT signatures (Supplementary Fig. S6A–S6E). However, the carcinoma components also had significantly higher EMT scores than the TCGA-OV cohort, suggesting that the OCS carcinoma component was either predisposed to undergo sarcomatous transformation or already transitioning to sarcoma ($P < 0.0001$; **Fig. 1C**).

To study the N-MYC/LIN28B pathway specifically, we analyzed *MYCN, LIN28B*, and *HMGA2* expression in the same dataset. *LIN28B* and *HMGA2* were significantly upregulated in carcinosarcomas compared with the TCGA-OV cohort ($P < 0.0001$ for both; **Fig. 1D**). As expected from the high EMT scores observed in the carcinomatous components, expressions of *LIN28B* and *HMGA2* were equally high in both components (Supplementary Fig. S6F).

p53 inhibition and upregulation of the N-MYC/LIN28B pathway in fallopian tube secretory epithelial cells gives rise to OCS

We established an OCS GEMM by directing both p53 inhibition and N-MYC/LIN28B pathway upregulation to the fallopian tube secretory

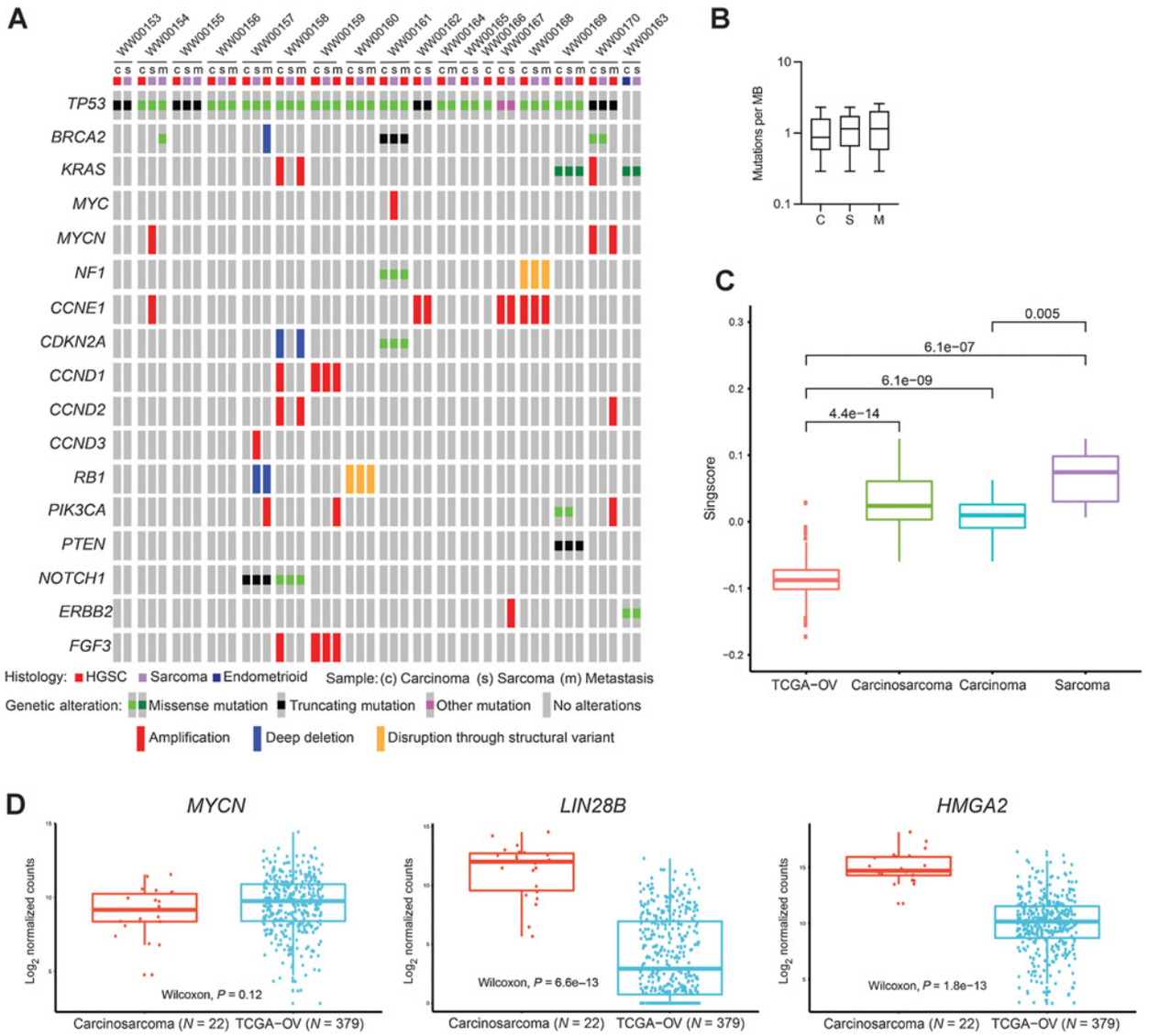

Figure 1.

Mutational and structural variant landscape of ovarian carcinosarcoma. **A,** Summary of frequently altered genes across the carcinoma, sarcoma, and metastasis samples from 18 macrodissected ovarian carcinosarcoma samples. For missense mutations, light green represents "unknown significance" and dark green represents "putative driver." Metastases are color-coded according to their histology. **B,** Mutation burden (mutations per megabase sequenced). **C,** Comparison of EMT scores in separated carcinomatous and sarcomatous regions from ovarian carcinosarcoma samples, whole ovarian carcinosarcoma tumors, and ovarian HGSC samples in TCGA. **D,** Expression of *MYCN*, *LIN28B*, and *HMGA2* in our ovarian carcinosarcoma cohort compared with ovarian HGSC tumors in TCGA. Data were analyzed using the nonparametric Wilcoxon rank-sum test. C, carcinoma; S, sarcoma; M, metastasis.

epithelial cell (FTSEC) via the *Pax8* promoter (Supplementary Fig. S7A). We included CRISPR-mediated knockout of *Pten* in subsequent lines, also giving rise to OCS (Supplementary Table S13). The initial founder tumor (T0) from a *Pax8-rtTA;TetO-Cre;LSL-Lin28b;SV40Tag* mouse, first passage tumors (T1), and a stable cell line derived from a T1 tumor (OCS GEMM cells) were validated by genotyping (Supplementary Tables S14 and S15).

Tumors expressed high levels of p53, as well as cytokeratin (pan-CK) in approximately 5% and vimentin in approximately 95% of the regions analyzed, indicating a predominantly sarcomatous phenotype (Supplementary Fig. S7B). Quantitative RT-PCR confirmed elevated expression of *Lin28b* in both the tumor and cell line (Supplementary Fig. S7C) and RNA-seq confirmed upregulation of *Lin28b* and *Mycn* in the tumors and upregulation of *Lin28b* and *Hmga2* in the cell line, relative to control fallopian tubes (Supplementary Fig. S7D; Supplementary Table S16).

GEMM tumors are resistant to current standard-of-care treatments but respond to the microtubule inhibitors vinorelbine and eribulin

We assessed the *in vivo* response of GEMM tumors to standard-of-care HGSC therapies, cisplatin, pegylated liposomal doxorubicin

(PLD), and paclitaxel. Overall, the tumors were refractory to all three treatments, as the time to progressive disease (PD) was the same as for vehicle treatment. PLD and cisplatin failed to demonstrate any meaningful response (**Fig. 2A**), although paclitaxel demonstrated modest responses with an increase in median time-to-harvest (TTH) from 15 to 36 days compared with vehicle treatment (**Table 1**, $P = 0.0101$, respectively). By contrast, significant tumor regression was observed in all tumors treated with the microtubule inhibitor vinorelbine, leading to improvement of median TTH [15 days (vehicle) vs. 81 days; **Fig. 2A**, **Table 1**; $P < 0.0001$]. Eribulin also resulted in significant tumor regression in all tumors, leading to improvement of median TTH (15 days vs. 46 days; **Fig. 2A**, **Table 1**; $P < 0.0001$). Expression of Ki67 in the tumors was significantly reduced one week after mice received a single dose of eribulin (**Fig. 2B**, $P < 0.001$).

Eribulin treatment reduces adhesion, invasion, and branching of the OCS GEMM cell line

In vitro functional assays showed eribulin reduced both adhesion to collagen matrices (**Fig. 2C**; $P = 0.024$) and invasion through extracellular matrices of OCS GEMM cells (**Fig. 2C**; $P = 0.0042$), compared with DMSO, and reduced branch formation in 3D collagen growth assays (**Fig. 2D**). Western blot analysis determined a reduction in expression of the mesenchymal markers ZEB1, N-cadherin, vimentin, and HMGA2 in OCS GEMM cells exposed to eribulin (**Fig. 2E**).

A cohort of OCS PDX models with N-MYC/LIN28B pathway upregulation recapitulates the biphasic and heterogeneous nature of OCS

We next expanded and characterized six PDX models of OCS with varying proportions of carcinoma and sarcoma, all harboring a mutation in *TP53* and other molecular features common to OCS (**Fig. 3A**; Supplementary Tables S17 and S18). Pan-cytokeratin and vimentin expression indicated the carcinomatous and sarcomatous components, respectively. Two models, PH142 and PH006, contained cells co-expressing pan-cytokeratin and vimentin, which were confirmed by a gynecological pathologist to have a mixed phenotype (**Fig. 3A**). The heterogeneous characteristics of the PDX cohort resembled the human OCS tumor landscape. Furthermore, all PDX models expressed HMGA2, suggesting that the N-MYC/LIN28B pathway was upregulated. Over time, a purely sarcomatous lineage (PH003sarc) arose from the original mixed PH003 model (called PH003mixed). RNA-seq data revealed that all PDX had higher HMGA2 expression and EMT scores than the epithelial ovarian cancer cohort TCGA-OV (**Fig. 3B** and **C**). The most sarcomatous PDX models (PH003sarc and PH592) had higher EMT scores than models containing regions of pure carcinoma (PH419 and PH003mixed). Interestingly, although all models had relatively high expression of *LIN28B*, only the more carcinomatous models expressed high levels of *MYCN* (PH419, PH142, and PH006), compared with the TCGA-OV cohort (**Fig. 3B**). By Western blot, expression of the mesenchymal markers ZEB1, N-cadherin and vimentin varied between models. There was a trend toward higher ZEB1 and vimentin expression in the more sarcomatous models, with the exception of PH003mixed, which expressed very low levels of ZEB1. N-cadherin was highly expressed in most models and HMGA2 was expressed at similar levels in all models (**Fig. 3D**). EMT scores were more representative of pathology (i.e., degree of mesenchymal characteristics) than any of the individual mesenchymal markers assessed by Western blotting.

Platinum-based chemotherapy is ineffective in OCS PDX

In vivo, 4/6 PDX were refractory to cisplatin, based on our previous criteria (**Fig. 4A**; Supplementary Fig. S8; ref. 40). Initial tumor regression was observed in PH142 and #1040 but PD occurred by days 42 and 60, respectively, defining both as cisplatin resistant (**Table 2**; ref. 40).

Microtubule-targeting agents paclitaxel, vinorelbine, and eribulin are effective in OCS

Microtubule-targeting agents induced tumor regression and showed an improvement of median TTH in most OCS PDX models. 3/6 PDX (#1040, PH419 and PH006) were classified as sensitive to paclitaxel according to the same criteria used for cisplatin (40), 2/6 were resistant (PH142 and PH592) and 1/6 was refractory (PH003; *in vivo* long-term treatment data were obtained for the PH003mixed model before development of the PH003sarc model; **Fig. 4A**; Supplementary Fig. S8). Indeed, 5/6 models displayed an improvement in median TTH compared with vehicle, with 4/6 models also displaying an improvement in median TTH compared with cisplatin (**Table 2**).

The same 3/6 OCS PDX (#1040, PH142, and PH006) were sensitive to vinorelbine, with 2/6 being resistant (PH419 and PH592) and PH003 again being refractory (**Fig. 4A**; Supplementary Fig. S8). The more sarcomatous PDX models, PH003 and PH592, were less sensitive to vinorelbine than the more carcinomatous models. Significant improvements in median TTH compared with vehicle were observed for 5/6 models, and in 4/6 models compared with cisplatin (**Table 2**).

Finally, the same 3/6 PDX models (#1040, PH419 and PH006) were sensitive to eribulin treatment, showing near complete responses. 2/6 were resistant (PH142 and PH592) and PH003 was again refractory (**Fig. 4A**; Supplementary Fig. S8). Significant improvements in median TTH compared with vehicle and cisplatin were observed for 5/6 and 4/6 models, respectively (**Table 2**). Eribulin treatment of PH592, which was predominantly sarcomatous, resulted in significant tumor stabilization to 40 days followed by marked tumor regression between days 60 to 80 before rapid disease progression. Even for the most aggressive model, PH003, eribulin treatment resulted in a statistically significant improvement in median TTH, albeit of short duration [8 days (vehicle) vs. 25 days (eribulin; $P = 0.0003$) and 15 days (cisplatin) vs. 25 days (eribulin; $P = 0.0044$; **Table 2**)].

Over time, a new lineage of the sarcomatous PDX PH592 (PH592-B) arose, which was markedly more sensitive to both cisplatin (median TTH of 15 days (PH592-A) versus 71 days (PH592-B); $P < 0.0001$) and eribulin (92 days (PH592-A) versus 102 days (PH592-B); $P = 0.0240$; Supplementary Fig. S9 and Supplementary Table S19) than the sister lineage PH592-A.

In vivo eribulin treatment reduces the expression of mesenchymal markers, including HMGA2, in OCS PDX tumors

PDX tumors were harvested one week after mice received a single dose of eribulin (or vehicle control) and expression of EMT markers was assessed by IHC and Western blot. Eribulin reduced expression of the mesenchymal marker HMGA2 as well as ZEB1 and N-cadherin in 6/7 and 5/7 models, respectively (**Fig. 4B–D**; Supplementary Fig. S10). Expression of ZEB1 was generally unchanged in 7/7 models following cisplatin treatment (Supplementary Fig. S11A).

Genes involved in cholesterol biosynthesis and immune recognition are differentially expressed in OCS PDX tumors following eribulin treatment

RNA-seq analysis of PDX tumors harvested one week after a single dose of eribulin (Supplementary Table S16) indicated significant

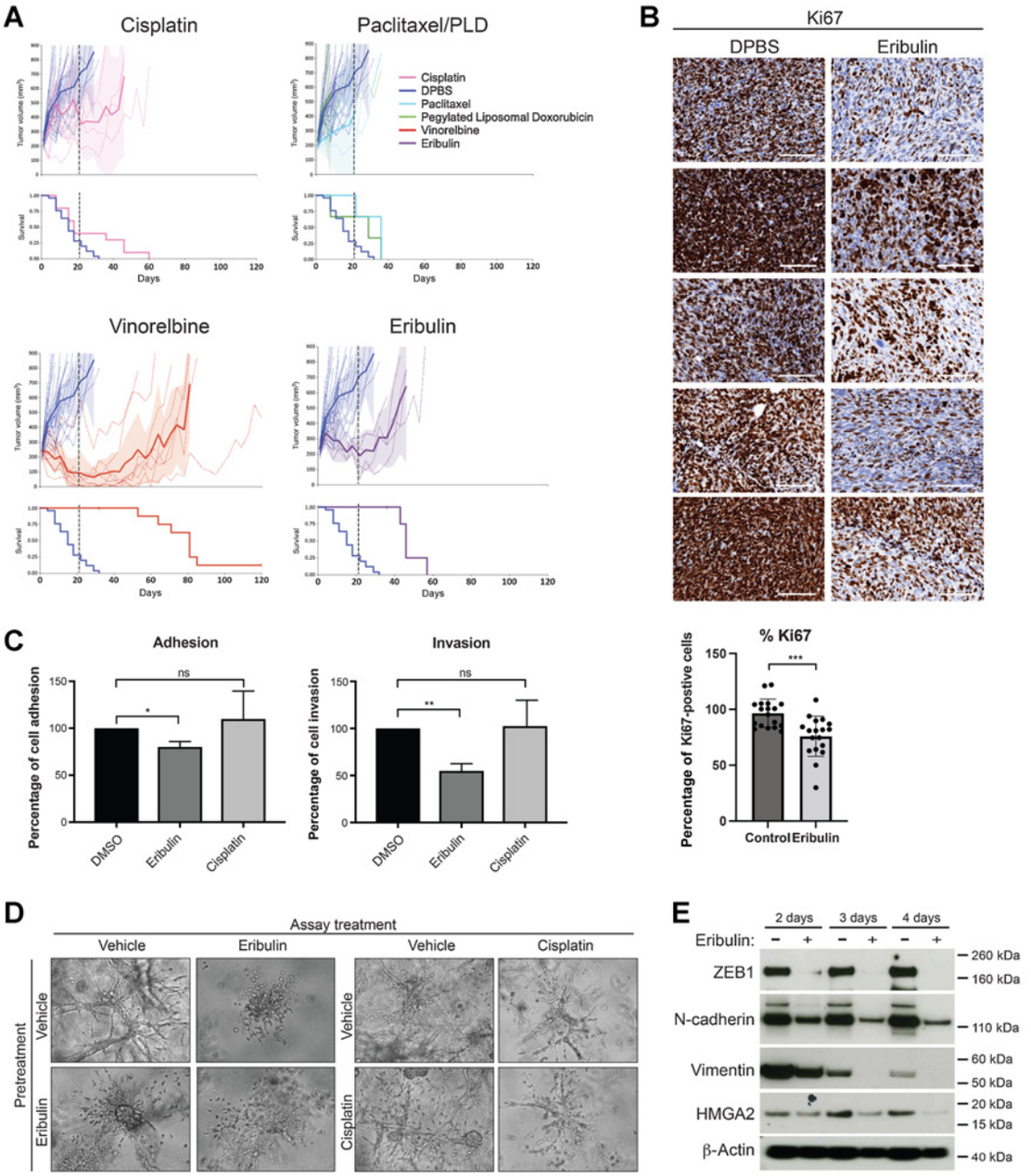

Figure 2.

GEMM OCS tumors were refractory to current standard-of-care treatments for ovarian cancer but were responsive to the microtubule drugs vinorelbine and eribulin. **A,** *In vivo* treatment of GEMM OCS tumors with DPBS ($n = 25$), cisplatin (4 mg/kg; $n = 10$), PLD (1.5 mg/kg; $n = 3$), paclitaxel (25 mg/kg; $n = 3$), vinorelbine (15 mg/kg; $n = 9$), and eribulin (1.5 mg/kg; $n = 5$). Dashed lines denote end of treatment period. Shaded area, 95% confidence interval. Time to PD and harvest is shown in **Table 1**. **B,** Representative images of Ki67 assessed by IHC in a number of tumors after a single dose of eribulin (or DPBS vehicle). Scale bars, 100 μm. The percentage of Ki67 cells was quantified in 6 fields of view per tumor. **C,** GEMM cells were pretreated with IC_{20} concentrations of eribulin (20 nmol/L) or cisplatin (0.2 μmol/L), or vehicle control (DMSO) for one week before being plated in adhesion assays (left) or migration and invasion assays (right). Percentage of adherent cells was calculated compared with vehicle-treated controls. Percentage of invading cells was calculated compared with number of migrating cells. Bar graphs represent the mean and SE across independent experimental repeats ($n = 3$–5). **D,** GEMM cells were pretreated as above with eribulin, cisplatin, or vehicle control (DMSO) for one week before being plated in collagen with treatment either removed or maintained. Representative images of colonies growing in collagen on day 8 are shown. Scale bars, 200 μm. **E,** Expression of the mesenchymal markers ZEB1, N-cadherin, vimentin, and HMGA2 in cells exposed to an IC_{50} concentration of eribulin (50 nmol/L) or DMSO control for the indicated time points was determined by Western blot analysis. β-Actin was used as a loading control. *, $P < 0.05$; **, $P < 0.01$; ***, $P < 0.001$; ns, nonsignificant.

Table 1. *In vivo* responses of GEMM tumors to cisplatin, paclitaxel, pegylated liposomal doxorubicin, vinorelbine, and eribulin.

Treatment	Number of mice (*n*)	Time to PD (d)	Media *n* TTH (d)	*P* value compared with vehicle	*P* value Compared with cisplatin	*P* value compared with eribulin	*P* value compared with paclitaxel	*P* value compared with PLD	*P* value compared with vinorelbine	Drug–response score
Vehicle	25	7	15							
Cisplatin	10	7	18	0.03		0.2	0.9	0.6	<0.0001	Refractory
Paclitaxel	3	7	36	0.01	0.9	0.007		0.5	0.0006	Refractory
PLD	3	7	29	0.08	0.6	0.004	0.5		0.0002	Refractory
Vinorelbine	9	56	81	<0.0001	<0.0001	0.001	0.0006	0.0002		Responsive
Eribulin	5	35	46	<0.0001	0.2		0.007	0.004	0.001	Responsive

Note: The GEMM tumors were refractory to cisplatin, paclitaxel, and PLD as the time to PD was the same as for vehicle-treated mice. PLD and cisplatin failed to produce any meaningful response with no significant difference in median TTH compared with vehicle treatment. Paclitaxel resulted in modest responses with an increase in median TTH from 15 to 36 days compared with vehicle-treated mice ($P = 0.01$). Improvements in time to PD were seen in tumors treated with vinorelbine (56 days) and eribulin (35 days). This led to a significant improvement of median TTH from 15 days for vehicle-treated mice to 81 days with vinorelbine ($P < 0.0001$) and to 46 days with eribulin ($P < 0.0001$). The log-rank test was used for statistical analysis of Kaplan–Meier survival curves (**Fig. 2A**).

downregulation of genes related to the Gene Ontology (GO) terms "protein targeting to membrane," "translational initiation," and "regulation of cholesterol biosynthesis," and upregulation of genes related to the GO term "immune activation" (**Fig. 5A**; Supplementary Tables S20–S23). Interestingly, significantly downregulated genes included twelve involved in cholesterol biosynthesis, cholesterol uptake or cholesterol transport: *SREBF2*, *HMGCR*, *HMGCS1*, *MVK*, *LDLR*, *INSIG1*, *IDI1*, *FDFT1*, *MSMO1*, *CYP51A1*, *SQLE*, and *STARD4*. Expression of hydroxymethylglutaryl-CoA synthase (HMGCS) and squalene epoxidase (SQLE), key components of the mevalonate (MVA) pathway involved in cholesterol biosynthesis, as well as the low-density lipoprotein receptor (LDLR), which mediates cellular uptake of exogenous cholesterol, was reduced in 4/7 models (PH419, PH142, PH592-A, and PH592-B) following eribulin treatment. Expression of SQLE was also significantly reduced in the PH003sarc model and N-MYC expression, which appears to indicate sensitivity to eribulin, was significantly reduced in 4/5 N-MYC–positive models following eribulin treatment (**Fig. 5B** and **C**). Interestingly, expression of HMGCS, SQLE, and LDLR was also reduced in 1/7 model (PH142) following cisplatin treatment. Unlike for eribulin treatment, this response was restricted to the PH142 model, with expression being generally unchanged in 6/7 models following cisplatin treatment (Supplementary Fig. S11A).

Eribulin treatment downregulates the mevalonate pathway and induces infiltration of CD8-positive T cells in OCS PDX models

To test whether cholesterol levels decreased in OCS tumors in response to eribulin treatment the amount of cholesterol was quantified in PDX tumors. Surprisingly, total cholesterol levels were found to increase almost 2-fold in 3/7 models (PH419, PH592-A, and PH592-B), and slightly in 2/7 models (PH142 and PH003sarc; **Fig. 5D**). The tumors with increased levels of cholesterol following eribulin treatment were the same tumors that displayed downregulation of the MVA pathway (**Fig. 5B** and **C**). Cholesterol levels were also significantly increased in 1/7 model (PH142) following cisplatin treatment, correlating with downregulation of the MVA pathway observed in this model (Supplementary Fig. S11B). Cholesterol levels were also slightly increased in PH419 tumors following cisplatin treatment, although not as dramatically as had been observed following eribulin treatment (Supplementary Fig. S11B). Total cellular cholesterol includes free cholesterol as well as cholesterol esters. In eribulin-responsive/N-MYC-positive PH419, increased total cholesterol was equally accounted for by both free cholesterol and cholesterol ester (**Fig. 5D**). Oil Red O staining indicated that eribulin-treated PH419 tumors had more esterified cholesterol within lipid deposits than did vehicle-treated tumors (**Fig. 5E**). Although a modest increase in lipid deposits were observed in PH142 tumors following both eribulin and cisplatin treatment, increases were more dramatic following eribulin treatment (Supplementary Fig. S11C). This effect was also specific to the models where increased cholesterol levels had previously been observed, as no increased lipid deposits were observed in PH006 tumors (Supplementary Fig. S11C).

To investigate this mechanism further, we generated a cell line from a PH419 tumor. Cells were plated on collagen, treated with eribulin, and harvested at indicated time-points. Expression of the mesenchymal markers ZEB1 and N-cadherin was reduced after four days of eribulin treatment and this effect was maintained at seven days (**Fig. 5F**). Expression of the early MVA pathway enzyme HMGCS was unaffected by eribulin treatment. In contrast, expression of the late MVA pathway enzyme SQLE, as well as the receptor for cholesterol uptake LDLR, was reduced after four days of eribulin treatment and this effect was maintained at seven days (**Fig. 5F**). Interestingly, total cholesterol levels were significantly increased 48 hours after eribulin treatment, confirming that MVA pathway downregulation occurred after cholesterol accumulation (**Fig. 5G**). We quantified cholesterol in a second cell line generated from a PH142 tumor with similar results (Supplementary Fig. S11D). As expected, on the basis of the results from the tumors, we also saw a maintained increase in cholesterol in PH142 cells following cisplatin treatment (Supplementary Fig. S11D).

To investigate cell death following treatment, we treated OCS cells with cisplatin or eribulin and harvested cells at 48 hours to look at the percentage of cells positive for Annexin V and/or PI. As was observed in the tumors, PH142 cells were more sensitive to cisplatin than PH419 cells (Supplementary Fig. S12A). Eribulin was unable to induce greater than 30% cell death in either cell line, even at doses more than 1,000-fold the dose that induced cholesterol accumulation (Supplementary Fig. S12A). Consequently, expression of cleaved PARP-1 and cleaved caspase-3 could be detected in cells treated with cisplatin but not those treated with eribulin (Supplementary Fig. S12B). Senescence assays were also carried out and indeed PH142 cells produced β-galactosidase following treatment with eribulin but not cisplatin (Supplementary Fig. S12C). Although PH419 cells did not produce

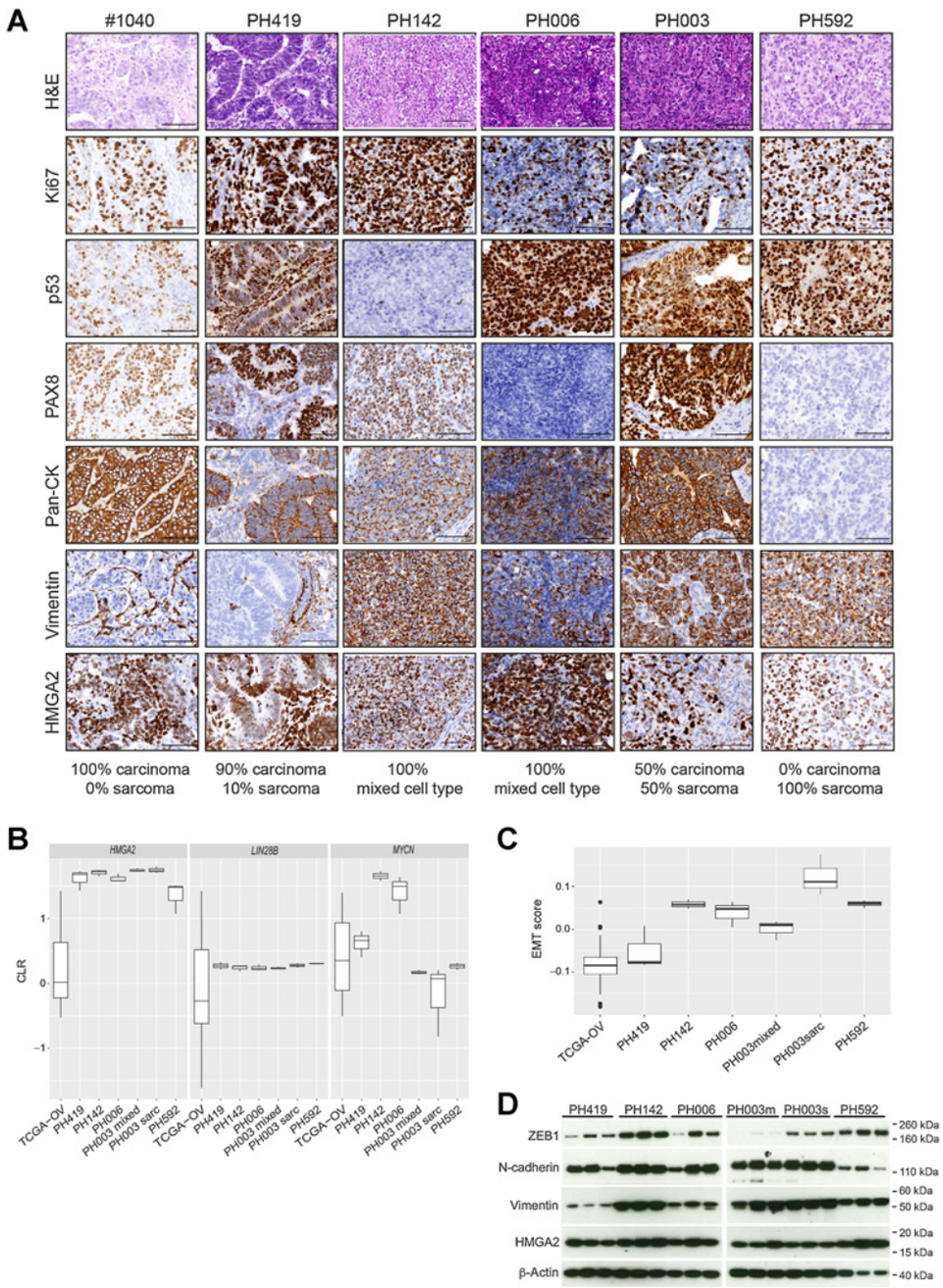

Figure 3.

Characterization of PDX models of OCS with varying proportions of carcinoma and sarcoma. **A,** Tumors from each PDX model of OCS were assessed by IHC. Representative images of H&E, Ki67, p53, PAX8, pan-CK, vimentin, and HMGA2 staining are shown. Scale bars, 100 μm. Proportions of carcinoma and sarcoma in each model, as assessed by a gynecological pathologist, are indicated below the images. #1040 and PH419 were almost purely carcinoma; PH142, PH006, and PH003 were mixed with both carcinomatous and sarcomatous characteristics (i.e., expressing both pan-CK and vimentin), and PH592 was purely sarcomatous, with some epithelial characteristics (i.e., pan-CK co-expression in some cells). **B,** Expression of *HMGA2, LIN28B*, and *MYCN* was determined from RNA-seq data for each OCS model ($n = 3$) compared with ovarian HGSC samples in TCGA ($n = 379$). **C,** EMT scores generated from RNA-seq data for tumors from each OCS PDX model are shown compared with EMT scores for ovarian HGSC samples in TCGA. **D,** Expression of the mesenchymal markers ZEB1, N-cadherin, vimentin, and HMGA2 in tumors from each OCS PDX model was determined by Western blot analysis. β-Actin was used as a loading control. CK, cytokeratin; CLR, centered log ratio; PH003m, PH003mixed; PH003s, PH003sarc.

β-galactosidase following eribulin treatment, they resembled senescent cells and appeared to have lost replicative capacity, a phenomenon we have previously observed in cancer cells treated with microtubule inhibitors (41).

Further analysis of the gene expression data obtained from the 18 cases in our OCS cohort, estimated they have fewer CD8-positive T cells than tumors in the TCGA-OV cohort (Supplementary Fig. S13). To investigate whether eribulin treatment could induce an immune response, as suggested by the gene expression data from the treated PDX models, we grew two additional OCS PDX models (#1105 and #1177) in mice harboring a human immune system (**Fig. 6A**; Supplementary Table S24). PDX tumors were harvested one week after mice received a single dose of eribulin, cisplatin or vehicle control, and CD8-positive T cells were detected by IHC (**Fig. 6B**). 2/2 models exposed to eribulin had a significantly greater percentage of CD8-positive T cells than control tumors ($P = 0.005$ and <0.0001 for #1105 and #1177, respectively; **Fig. 6C**). A significant increase in the percentage of CD8-positive T cells was also observed following cisplatin treatment in 1/2 models (#1105, $P < 0.0001$; **Fig. 6C**).

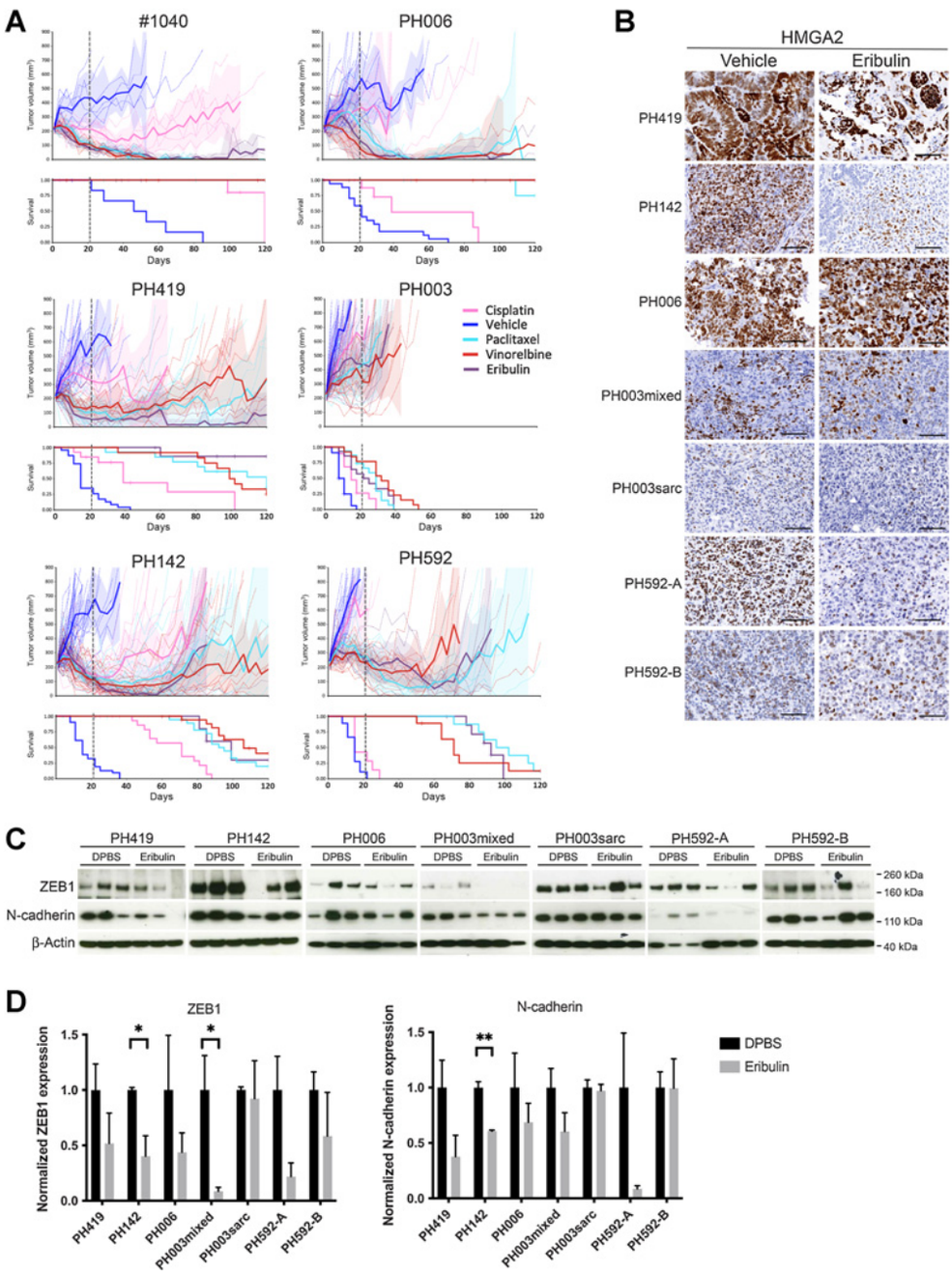

Figure 4.

PDX OCS tumors were refractory to cisplatin but displayed mostly impressive responses to microtubule drugs. **A,** *In vivo* treatment of OCS PDX tumors with DPBS, cisplatin (4 mg/kg), paclitaxel (25 mg/kg), vinorelbine (15 mg/kg), and eribulin (1.5 mg/kg, with the exception of mice harboring #1040 tumors, which received doses of 1 mg/kg). *n* values for each model are shown in **Table 2**. Dashed lines, end of treatment period. Shaded area, 95% confidence interval. More carcinomatous models are shown on the top left and the more sarcomatous models on the bottom right. Time to PD and harvest are shown in **Table 2**. **B,** Expression of HMGA2 in tumors from each OCS PDX model after a single dose of vehicle (DPBS) or eribulin was determined by IHC. Scale bars, 100 μm. **C,** Expression of the mesenchymal markers ZEB1 and N-cadherin in tumors from each OCS PDX model after a single dose of vehicle (DPBS) or eribulin was determined by Western blot analysis. β-Actin was used as a loading control. **D,** Quantification of expression data in **C**. *, $P < 0.05$; **, $P < 0.01$.

Table 2. *In vivo* responses of OCS PDXs to cisplatin, paclitaxel, vinorelbine, and eribulin.

PDX model	Treatment	Number of mice (*n*)	Time to PD (days)	Median TTH (d)	*P* value compared with vehicle	*P* value compared with cisplatin	*P* value compared with eribulin	*P* value compared with paclitaxel	*P* value compared with vinorelbine	Drug–response score (Topp et al.)
#1040	Vehicle	8	7	53						
	Cisplatin	8	60	120	0.0008					Resistant
	Eribulin	7	>120	>120	0.002	0.1		>1	>1	Sensitive
	Paclitaxel	7	>120	>120	0.001	0.1	>1		>1	Sensitive
	Vinorelbine	6	>120	>120	0.003	0.1	>0.1	>1		Sensitive
PH419	Vehicle	23	7	15						
	Cisplatin	13	7	39	<0.0001					Refractory
	Eribulin	8	>120	>120	<0.0001	0.002		0.09	0.04	Sensitive
	Paclitaxel	14	112	120	<0.0001	0.004	0.09		0.6	Sensitive
	Vinorelbine	12	80	99	<0.0001	0.02	0.04	0.6		Resistant
PH142	Vehicle	31	7	15						
	Cisplatin	19	42	71	<0.0001					Resistant
	Eribulin	10	77	99	<0.0001	0.004		0.8	0.4	Resistant
	Paclitaxel	22	57	95	<0.0001	<0.0001	0.8		0.1	Resistant
	Vinorelbine	19	120	106	<0.0001	<0.0001	0.4	0.1		Sensitive
PH006	Vehicle	17	7	22						
	Cisplatin	9	7	39	0.006					Refractory
	Eribulin	6	>120	>120	0.0005	0.008		0.5	>1	Sensitive
	Paclitaxel	7	>120	>120	<0.0001	0.002	0.5		0.3	Sensitive
	Vinorelbine	7	>120	>120	<0.0001	0.001	>1	0.3		Sensitive
PH003	Vehicle	23	7	8						
	Cisplatin	19	7	15	0.0005					Refractory
	Eribulin	14	7	25	0.0003	0.004		1	0.1	Refractory
	Paclitaxel	16	7	29	<0.0001	0.003	1		0.07	Refractory
	Vinorelbine	13	18	32	<0.0001	0.0005	0.1	0.07		Refractory
PH592	Vehicle	18	7	15						
	Cisplatin	7	7	15	0.03					Refractory
	Eribulin	8	80	92	<0.0001	<0.0001		0.3	0.3	Resistant
	Paclitaxel	8	88	102	<0.0001	<0.0001	0.3		0.2	Resistant
	Vinorelbine	9	63	71	<0.0001	<0.0001	0.3	0.2		Resistant

Note: Cisplatin failed to achieve any meaningful tumor response in four of six PDX models; PH419, PH006, PH003, and PH592. PH142 and #1040 demonstrated some response to cisplatin with improvement of median TTH from 15 to 71 days ($P < 0.0001$) and 53 to 120 days ($P = 0.0008$), compared with vehicle-treated mice, respectively. However, times to PD were less than 100 days (PH142 at 42 days and #1040 at 60 days), therefore these tumors were classified as resistant to cisplatin. Three of six PDXs (#1040, PH419, and PH006) were shown to be sensitive to paclitaxel *in vivo*, two PDXs (PH142 and PH592) were resistant, and one PDX (PH003) was refractory based on the same *in vivo* drug response score as cisplatin. Three of six OCS PDXs (#1040, PH142, and PH006) were sensitive, two PDXs (PH419 and PH592) were resistant, and one PDX (PH003) was refractory to vinorelbine treatment. Three of six OCS PDX models (#1040, PH419, and PH006) were sensitive, two PDXs (PH412 and PH592) were resistant, and one PDX (PH003) was refractory to eribulin treatment. Significant improvements in median TTH compared with cisplatin-treated mice were observed for four models [39 to >120 days for PH419 ($P = 0.002$), 71 to 99 days for PH142 ($P = 0.004$), 39 to >120 days for PH006 ($P = 0.008$), 15 to 25 days for PH003 ($P = 0.004$), and 15 to 92 days for PH592 ($P < 0.0001$)]. The log-rank test was used for statistical analysis of Kaplan–Meier survival curves (**Fig. 4A**).

Discussion

OCS is a rare, heterogeneous and clinically aggressive cancer, with poorer OS than HGSC despite a similar mutation and copy-number profile (42). The biphasic nature of OCS and a poor understanding of how these tumors develop have hindered development of effective treatment options. Two recent studies performed WES on separated components of OCS tumors, but on no more than four tumors each (8, 9). Here, we analyzed 377 genes (for mutations, copy number, or both) in 18 OCS tumors where the carcinomatous and sarcomatous components were analyzed independently along with associated metastases, where available. We found mutations commonly identified in OCS, with the initial or truncal mutation likely to occur in *TP53*. In all of the cases, the same *TP53* mutation was identified in all sites available; carcinoma, sarcoma and metastasis, suggesting strongly that OCS tumors in our cohort were monoclonal. Furthermore, we carried out RNA-seq analysis, which has not previously been achieved for the independent components in OCS. The carcinomatous component was found to have a significantly higher EMT score than conventional HGSC, indicating that these tumors may have been primed to undergo sarcomatous transformation early in carcinogenesis. Together, these data indicate that EMT plays a key role in OCS tumorigenesis and support the conversion theory for OCS histogenesis. This study also highlights the potential downfall of treating women with OCS in the same way as HGSC, as we have shown that despite the genomic similarity, OCS are phenotypically distinct, particularly with regard to drug responses and mesenchymal characteristics.

Significant upregulation of *LIN28B* and *HMGA2* in our cohort of 18 OCS tumors compared with HGSC suggests that the N-MYC/LIN28B pathway is important in the development and maintenance of OCS. Using this knowledge, we developed a GEMM of OCS by overexpressing *Lin28b* and inhibiting p53 in PAX8$^+$ FTSECs. Although the OCS

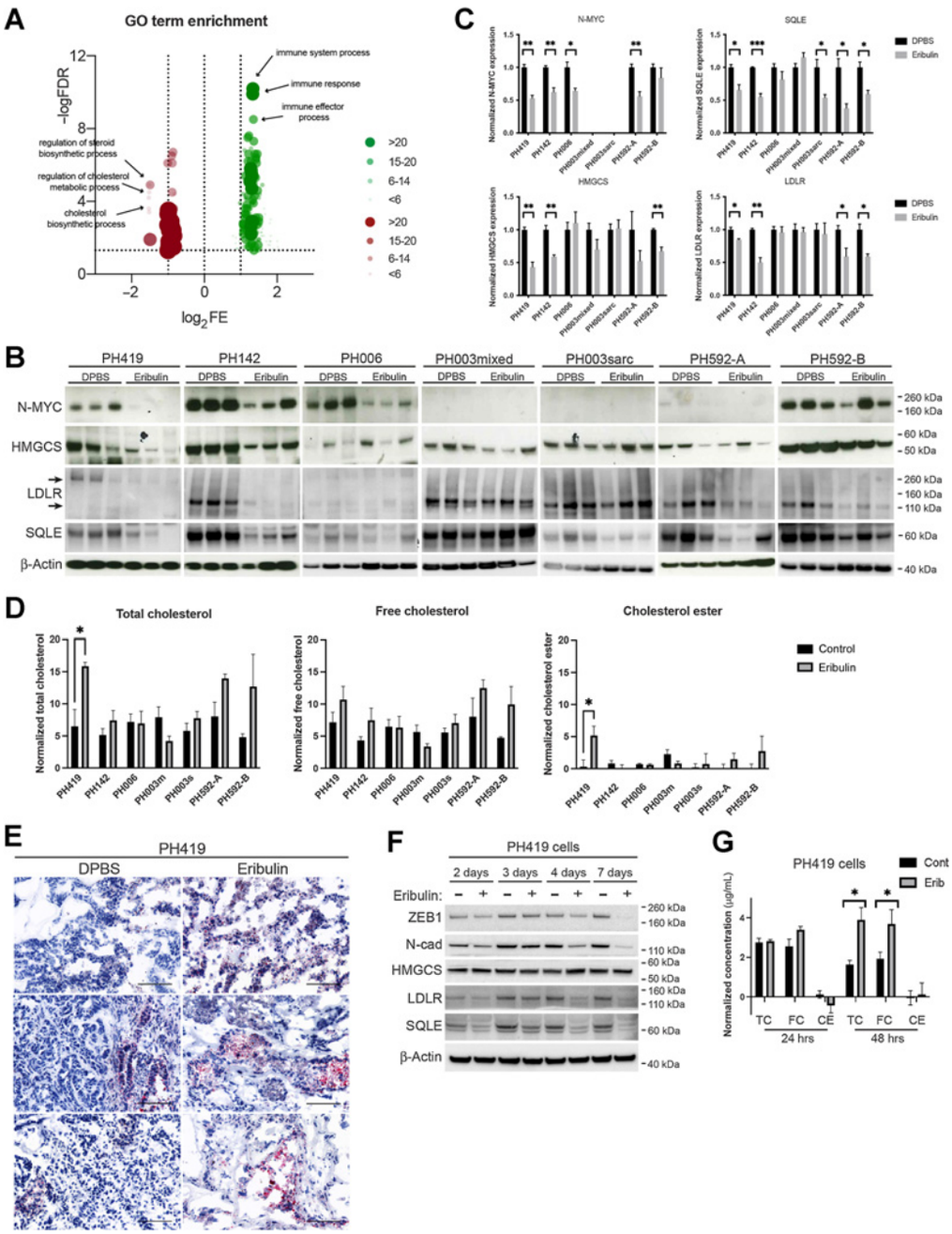

Figure 5.

The mevalonate pathway was downregulated following eribulin treatment of OCS cells and tumors as a result of increased cellular cholesterol. **A,** Analysis of GO terms enriched for downregulated (left) and upregulated (right) differentially expressed genes. Circle sizes indicate differentially expressed genes present in each GO term. Differentially expressed genes are listed in Supplementary Tables S20–S23. **B,** Expression of N-MYC, HMGCS, SQLE, and LDLR in tumors from each OCS PDX model after a single dose of vehicle (DPBS) or eribulin was determined by Western blot analysis. β-Actin was used as a loading control. **C,** Quantification of expression data in **B**. **D,** Quantification of total cholesterol, free cholesterol, and cholesterol ester in tumors from each OCS PDX model after a single dose of vehicle (DPBS) or eribulin. **E,** Representative images of Oil Red O staining in PH419 tumors following a single dose of vehicle (DPBS) or eribulin. Scale bar, 100 μm. **F,** Expression of the mesenchymal markers ZEB1 and N-cadherin, as well as the MVA pathway proteins HMGCS, SQLE, and LDLR, in PH419 cells exposed to 15 nmol/L of eribulin or DMSO control for the indicated time points was determined by Western blot analysis. β-Actin was used as a loading control. **G,** Quantification of total cholesterol, free cholesterol, and cholesterol ester in PH419 cells exposed to 15 nmol/L of eribulin or DMSO control for the indicated time points. Bar graphs represent the mean and SE across independent experimental repeats ($n = 3$). *, $P < 0.05$; **, $P < 0.01$; ***, $P < 0.001$. TC, total cholesterol; FC, free cholesterol; CE, cholesterol ester.

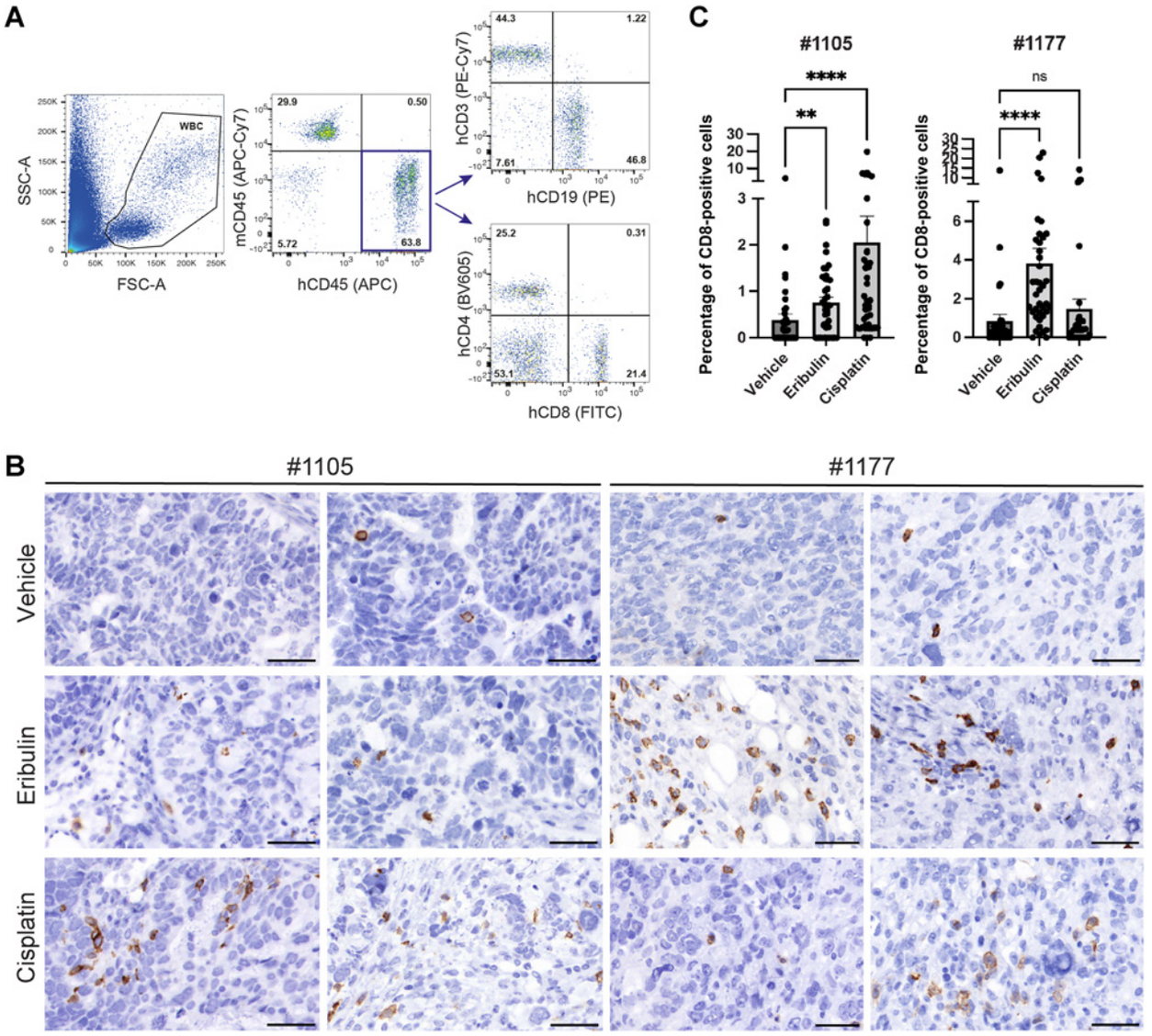

Figure 6.

PDX tumors have a greater percentage of human CD8-positive T cells following eribulin treatment. **A,** Blood from NSG mice reconstituted with human CD34$^+$ hematoietic stem cells was analyzed 12 weeks post-reconstitution by flow cytometry to determine proportion of human immune cells present. **B,** PDX tumors harvested one week after mice received a single dose of vehicle (DPBS), eribulin (3 mg/kg), or cisplatin (4 mg/kg) were analyzed by IHC. Representative images of tumor-infiltrating CD8-positive T cells are shown for each model and treatment. Scale bar, 50 μm. **C,** Percentage of CD8-positive T cells was quantified in 20 fields of view at ×400 magnification for each tumor and is shown for individual mice. Statistical analysis was performed using the Kruskal–Wallis test. **, $P < 0.01$; ****, $P < 0.0001$; ns, nonsignificant.

GEMM tumors exhibited high expression of *Lin28b* and *Mycn*, the derived cell line displayed high expression of *Lin28b* and *Hmga2*, indicating that we had generated two closely related preclinical models of OCS. This demonstrates the complexity of the N-MYC pathway, as was also indicated by the RNA-seq data from our patient samples. Observed expression of this pathway depends on multiple feedback loops and influences from outside the pathway, such as by transcription factors, with influences occurring at the level of transcription and translation, frequently resulting in complex relationships (43).

These models were used to compare the current standard-of-care treatments for OCS with novel treatments, including the unique microtubule-targeting drug eribulin, which has been shown to reverse EMT (29) and has demonstrated efficacy against metastatic breast cancer, soft-tissue sarcoma and NSCLC (30–33). Although the GEMM tumors were refractory to cisplatin, paclitaxel and PLD *in vivo*, they were responsive to vinorelbine and eribulin. After just a single dose of eribulin, a notable decrease in tumor cell proliferation was observed. *In vitro*, eribulin significantly reduced adhesion, invasion and branching in 3D cultures. Finally, an impressive reduction in expression of the mesenchymal markers HMGA2, ZEB1, N-cadherin, and vimentin was observed in GEMM cells, indicating that eribulin could reverse EMT in these cells.

A cohort of molecularly annotated OCS PDX models was found to have higher EMT scores than HGSC with the most carcinomatous model, PH419, having the lowest EMT score and the most sarcomatous model, PH003sarc, having the highest. At the protein level, PH003sarc also had the highest expression of the mesenchymal markers N-cadherin and vimentin. Interestingly, the two models containing mixed cells, PH142 and PH006, also had high expression of N-cadherin, vimentin and ZEB1. This matched their high EMT scores obtained from RNA-seq data and indicated that pathology alone was insufficient to determine the level of sarcomatous transformation occurring in each OCS model.

Anti-microtubule agents were more effective than platinum-based chemotherapy in our OCS PDX cohort. The proportion of carcinoma correlated with cisplatin sensitivity, where the more carcinomatous PDX had some initial response, whereas the most sarcomatous PDX were completely refractory. Responses were observed for almost all PDX to the microtubule-targeting drugs paclitaxel, vinorelbine, and eribulin. With metastases more commonly comprising carcinoma cells, this suggests that eribulin would also inhibit progression and metastasis. PDX PH003 was the exception, where tumors were refractory to all treatment regimens tested. This drug-refractory PDX was found to lack N-MYC expression, representing a particularly aggressive subtype of OCS, corresponding to rapid PD in the patient (44). PH952-A, the more drug-resistant lineage of PH592, had almost undetectable levels of N-MYC, whereas it was expressed in the more drug-sensitive lineage, PH592-B, supporting our hypothesis that N-MYC correlates with sensitivity to eribulin. We observed a decrease in HMGA2, N-cadherin and ZEB1 expression in most models following a single dose of eribulin. We hypothesized that eribulin interfered with the N-MYC pathway, leading to a reduction in the mesenchymal characteristics of OCS, including downregulation of HMGA2. Indeed, we later discovered that eribulin reduced the expression of N-MYC in N-MYC-expressing tumors, with the exception of PH592-B. As has been seen for MYC (45, 46), we hypothesize that N-MYC associates with microtubules to facilitate nuclear translocation and stabilization, which may be affected by microtubule inhibitors, such as eribulin. Despite PH419 being the most carcinomatous model, it was still found to express the mesenchymal markers ZEB1, N-cadherin, and HMGA2, which were all reduced following eribulin treatment. This model was also found to have a higher EMT score than most HGSC tumors, and so it was not surprising that this model was also significantly sensitive to eribulin treatment. Ultimately, we found eribulin to be very effective in most of our OCS models, indicating that it should be offered to patients with OCS as an alternative therapeutic to carboplatin and paclitaxel. As has been seen in locally advanced and metastatic breast cancer (47), we hypothesize that eribulin will improve survival of OCS patients with a manageable toxicity profile.

We found that eribulin treatment also resulted in a significant reduction in the expression of genes in the MVA pathway and a significant upregulation of genes involved in immune activation. Activation of the MVA pathway has previously been observed in *MYCN* amplified neuroblastoma, with apparent reliance of these tumors on this pathway for survival (48). We hypothesize that N-MYC is a key driver of OCS, implicating the MVA pathway in OCS cell survival and drug resistance. Notably, the most aggressive PDX model PH003mixed, which displayed no change in expression of MVA pathway proteins after eribulin treatment, also had very low expression of *MYCN* by RNA-seq and expression of N-MYC was undetectable by Western blot, further supporting our hypothesis that N-MYC expression confers sensitivity to eribulin. On the other hand, one of the most sensitive PDX models PH006, which also displayed no change in expression of MVA pathway proteins after eribulin treatment, had very high expression of N-MYC by RNA-seq and Western blot. It is possible that changes in cholesterol levels and MVA pathway activity in this model may be evident at another time-point. Supporting the RNA-seq data, we saw a reduction in the expression of HMGCS, SQLE, and LDLR in 4/7 PDX models: PH419, PH142, PH592-A, and PH592-B. SQLE expression was also reduced in the PH003sarc model. Strikingly, cholesterol levels were increased in the 4/7 PDX in which we had observed a downregulation of MVA pathway proteins. Previously, a study of drugs that could inhibit EMT in breast cancer cells also observed an increase in cellular cholesterol levels following treatment (49). Increased intracellular cholesterol was found to reduce membrane fluidity, leading to a reversal of EMT characteristics, as we have observed in this study. Although cholesterol plays an important role in regulating the properties of cell membranes, too much cellular cholesterol can also be toxic (50). We hypothesized that as cholesterol reached toxic levels as a result of eribulin treatment, negative feedback regulation of the MVA pathway took place to lower cholesterol levels. This downregulation of the MVA pathway is of particular interest, as it has previously been associated with an improved response to anticancer drugs and reduced development of drug resistance (reviewed in ref. 51). We confirmed this order of events using a PH419 primary cell line, where cholesterol levels were significantly increased 48 hours after eribulin treatment, resulting in reduced EMT indicated by a decreased expression of ZEB1 and N-cadherin, and followed by downregulation of SQLE and LDLR expression at 96 hours. With respect to OCS, this protective response may come too late, with cell death, growth inhibition, and tumor regression resulting from eribulin treatment in many cases. We also observed significantly increased cholesterol accumulation following cisplatin treatment in the PH142 model. Interestingly, this model is the most sensitive to cisplatin treatment, likely due to harboring a *BRCA2* mutation. Although cholesterol accumulation and subsequent MVA pathway downregulation occurred when OCS responded to other anticancer drugs, such as cisplatin, this process was more striking following eribulin treatment. Importantly, EMT reversal was not observed following cisplatin treatment, and tumor remission was not as deep or as long-lasting compared with eribulin treatment.

Cholesterol accumulation has been found to induce an immune response in cancer via multiple mechanisms, such as through enhancing inflammation signaling pathways or inducing antigen presentation (52). Indeed, in our OCS PDX models, we also observed a significant increase in the expression of genes involved in immune responses following eribulin treatment, such as *TLR7* and *IRF8*, which have independently been associated with increased inflammation and recruitment of tumor-infiltrating lymphocytes in different cancer types (53, 54). Indeed, we observed increased numbers of CD8-positive T cells in tumors following eribulin treatment, indicating activation of an immune response. Furthermore, a recent study linked *MYCN* overexpression in neuroblastoma to cancer immune evasion (55). Thus, we have found that eribulin can initiate antitumor immune responses in OCS, as has been observed in other tumor types treated with eribulin (56). We have also discovered that OCS tumors that are sensitive to eribulin treatment exhibit an accumulation of cholesterol, which may be responsible for instigating these observed immune responses. Ultimately, we hypothesize that eribulin elicits its strong antitumor effects in OCS through a combination of EMT reversal, MVA pathway downregulation and induction of an immune response.

Therefore, early-phase clinical trials in OCS of eribulin as a single agent or in combination with immunotherapy should be initiated to improve treatment options for women with OCS.

Authors' Disclosures

E.L. Kyran reports grants from Stafford Fox Medical Research Foundation and personal fees from Cancer Research UK Cambridge Institute Studentship, Cambridge Australia Poynton Scholarship, and Cambridge Trust International Scholarship during the conduct of the study. M.J. Wakefield reports grants from National Health and Medical Research Council during the conduct of the study and other support from Clovis outside the submitted work. C.J. Vandenberg reports grants from The Stafford Fox Medical Research Foundation and Cancer Council Victoria during the conduct of the study. A. Hadla reports other support from University of Melbourne during the conduct of the study. G. Dall reports grants from Victorian Cancer Agency during the conduct of the study and from Australian and New Zealand Gynecological Oncology Group outside the submitted work. O. Kondrashova reports personal fees from XING Technologies outside the submitted work. R. Upstill-Goddard reports grants from Cancer Research UK and Beatson Institute, Glasgow during the conduct of the study. R. Glasspool reports grants from Boehringer Ingelheim and Clovis Oncology, nonfinancial support from GSK, other support from Novartis, and personal fees from Clovis Oncology, GSK, AstraZeneca, Immunogen, MSD, and Sotio outside the submitted work. A.V. Biankin reports personal and institutional financial interest in BMS, AstraZeneca, and MyTomorrows; leadership role and stock ownership in Cumulus Oncology, Modulus Oncology, Wollemia Oncology, concr, Cambridge Cancer Genomics, Gabriel Precision Oncology, and human.ai; and IP/financial interest in Agilent Technologies. N. Traficante reports grants from AstraZeneca Pty. Ltd. outside the submitted work. A. DeFazio reports grants from AstraZeneca outside the submitted work. D.D. Bowtell reports grants from Genentech Roche, Beigene, and AstraZeneca, and personal fees from Exo Therapeutics outside the submitted work. I.A. McNeish grants and personal fees from AstraZeneca, and personal fees from Clovis Oncology, GSK, Roche, Epsila Bio, and ScanCell outside the submitted work. C.L. Scott reports grants and other support from Australian Cancer Research Foundation and National Health and Medical Research Council (NHMRC Australia), other support from Victorian State Government Operational Infrastructure Support, nonfinancial support from Eisai Inc., and grants from The Stafford Fox Medical Research Foundation, Cancer Council Victoria, Victorian Cancer Agency, Herman Trust University of Melbourne, and CRC Cancer Therapeutics during the conduct of the study. C.L. Scott also reports nonfinancial support from Clovis Oncology and Beigene, grants and other support from Eisai Inc., AstraZeneca, and Sierra Oncology Inc., grants from Boehringer Ingelheim, other support from Roche and Takeda, and nonfinancial support and other support from MSD outside the submitted work. H.E. Barker reports grants from Cancer Council Victoria and other support from Stafford Fox Medical Research Foundation and Eisai during the conduct of the study; other support from Eisai, Clovis, AstraZeneca, Sierra Oncology Inc., MSD, and Boeringer Ingelheim outside the submitted work. No disclosures were reported by the other authors.

Authors' Contributions

G.Y. Ho: Conceptualization, resources, data curation, software, formal analysis, validation, investigation, visualization, methodology, writing–original draft, writing–review and editing. **E.L. Kyran:** Data curation, formal analysis, validation, investigation, visualization, methodology, writing–original draft, writing–review and editing. **J. Bedo:** Resources, data curation, software, formal analysis, supervision, validation, investigation, visualization, methodology, writing–review and editing. **M.J. Wakefield:** Resources, data curation, software, formal analysis, supervision, validation, investigation, visualization, methodology, writing–review and editing. **D.P. Ennis:** Conceptualization, data curation, formal analysis, validation, investigation, visualization, writing–review and editing. **H.B. Mirza:** Data curation, software, formal analysis, validation, investigation, visualization, methodology, writing–review and editing. **C.J. Vandenberg:** Resources, data curation, formal analysis, supervision, investigation, visualization, writing–review and editing. **E. Lieschke:** Resources, data curation, formal analysis, investigation, visualization, writing–review and editing. **A. Farrell:** Formal analysis, investigation, writing–review and editing. **A. Hadla:** Formal analysis, investigation, writing–review and editing. **R. Lim:** Data curation, visualization, writing–review and editing. **G. Dall:** Resources, writing–review and editing. **J.E. Vince:** Formal analysis, investigation, writing–review and editing. **N.K. Chua:** Formal analysis, writing–review and editing. **O. Kondrashova:** Data curation, methodology, writing–review and editing. **R. Upstill-Goddard:** Conceptualization, data curation, investigation, writing–review and editing. **U.-M. Bailey:** Conceptualization, data curation, investigation, writing–review and editing. **S. Dowson:** Conceptualization, data curation, writing–review and editing. **P. Roxburgh:** Conceptualization, data curation, writing–review and editing. **R.M. Glasspool:** Conceptualization, data curation, writing–review and editing. **G. Bryson:** Conceptualization, data curation, writing–review and editing. **A.V. Biankin:** Supervision, writing–review and editing. **S.L. Cooke:** Conceptualization, formal analysis, supervision, methodology, writing–review and editing. **G. Ratnayake:** Data curation, formal analysis, writing–review and editing. **O. McNally:** Resources, supervision, writing–review and editing. **N. Traficante:** Resources, writing–review and editing. **A. DeFazio:** Formal analysis, supervision, writing–review and editing. **S.J. Weroha:** Resources, formal analysis, writing–review and editing. **D.D. Bowtell:** Formal analysis, supervision, writing–review and editing. **I.A. McNeish:** Conceptualization, resources, data curation, software, formal analysis, supervision, funding acquisition, validation, investigation, visualization, methodology, writing–original draft, project administration, writing–review and editing. **A.T. Papenfuss:** Conceptualization, resources, software, formal analysis, supervision, funding acquisition, validation, visualization, methodology, project administration, writing–review and editing. **C.L. Scott:** Conceptualization, resources, data curation, formal analysis, supervision, funding acquisition, validation, investigation, visualization, methodology, writing–original draft, project administration, writing–review and editing. **H.E. Barker:** Conceptualization, resources, data curation, software, formal analysis, supervision, funding acquisition, validation, investigation, visualization, methodology, writing–original draft, project administration, writing–review and editing.

Acknowledgments

This work was supported by fellowships and grants from the National Health and Medical Research Council (NHMRC Australia; project grants 1062702, 1081178 to C.L. Scott, and 1104348 to M.J. Wakefield, D.D. Bowtell, A.T. Papenfuss, and C. L. Scott, Senior Research Fellowship 1116955 (to A.T. Papenfuss), Investigator grant 2008692 (to J.E. Vince), Ideas grant 1183070 (to J.E. Vince); the Stafford Fox Medical Research Foundation (to E.L. Kyran, J. Bedo, C.J. Vandenberg, R. Lim, A.T. Papenfuss, C.L. Scott, and H.E. Barker); the Lorenzo and Pamela Galli Medical Research Trust (to A.T. Papenfuss); Cancer Council Victoria (Sir Edward Dunlop Fellowship in Cancer Research to C.L. Scott and Ovarian Cancer Research grant-in-aid 1186314 to G. Ratnayake, C.J. Vandenberg, A. Farrell, and H.E. Barker); the Victorian Cancer Agency (Clinical Fellowships CRF10–20, CRF16014 to C.L. Scott and Early Career Research Fellowship ECRF19003 to G. Dall); Herman Trust University of Melbourne (to C.L. Scott); CRC Cancer Therapeutics (grant support to C.L. Scott and PhD top-up scholarship to G.Y. Ho); Australian Commonwealth Government and the University of Melbourne (Research Training Program Scholarship to G.Y. Ho and A. Hadla); Cancer Research UK Cambridge Institute Studentship; Cambridge Poynton Scholarship; Cambridge Trust International Scholarship (PhD funding for E.L. Kyran); research funding from Eisai (to C.L. Scott and H.E. Barker). The Scottish Genomes Partnership is funded by the Chief Scientist Office of the Scottish Government Health Directorates (grant reference SGP/1) and The Medical Research Council Whole Genome Sequencing for Health and Wealth Initiative. Additional funding was provided by the Medical Research Council (the Glasgow Molecular Pathology Node, grant reference MR/N005813/1), Cancer Research UK (grant references A15973 to I.A. McNeisho and A17263 to A.V. Biankin), the Wellcome Trust (grant reference 103721/Z/14/Z to A.V. Biankin), and the Beatson Cancer Charity (grant reference 15–16–051 to I.A. McNeish and P. Roxburgh), the Imperial NIHR Biomedical Research Centre (grant references PSC593 and P77646 to I.A. McNeish, D.P. Ennis, and H.E. Barker), and Ovarian Cancer Action (grant reference P76567 to I.A. McNeish, D.P. Ennis, and H.E. Barker). The authors thank Silvia Stoev, Rachel Hancock, and Kathy Barber for technical assistance. They thank Profs. Ronny Drapkin and Jane Visvader and Osaka Bioscience Institute, Japan, and Prof. Johannes H. Schulte for kind gifts of the mouse strains used to generate the GEMM. The authors thank Dr. P. Haluska (Mayo Clinic) for the cryopreserved PDX material used to re-establish PDXs PH419, PH142, PH006, PH003, and PH592 within their laboratory. They thank Eisai Co., Ltd., for supply of eribulin. The authors thank Prof. Elizabeth Swisher and Dr. M. Radke for the BROCA sequencing of case #1040, Prof. Sean Grimmond and Dr. J. Vissers for WGS of cases #1105 and #1177, and Andrew Fellowes for the TSO500 sequencing of cases PH142, PH003, and PH006. They thank Jocelyn Penington for data deposition to EGA. This work was made possible through the Australian Cancer Research Foundation, the Victorian State Government Operational Infrastructure Support,

and Australian Government NHMRC IRIISS. The Australian Ovarian Cancer Study Group was supported by the U.S. Army Medical Research and Materiel Command under DAMD17–01–1-0729, The Cancer Council Victoria, Queensland Cancer Fund, The Cancer Council New South Wales, The Cancer Council South Australia, The Cancer Council Tasmania and The Cancer Foundation of Western Australia (Multi-State Applications 191, 211, and 182), and the National Health and Medical Research Council of Australia (NHMRC; ID199600, ID400413, and ID400281). The Australian Ovarian Cancer Study gratefully acknowledges additional support from Ovarian Cancer Australia and the Peter MacCallum Foundation. The AOCS also acknowledges the cooperation of the participating institutions in Australia and acknowledges the contribution of the study nurses, research assistants, and all clinical and scientific collaborators to the study. The complete AOCS Study Group can be found at www.aocstudy.org. Support was also provided by Ovarian Cancer Action, the Cancer Research UK Centres and Experimental Cancer Medicine Centres at both Glasgow and Imperial and the NIHR Imperial Biomedical Research Centre. The authors would like to thank all of the women who participated in these research programs.

The publication costs of this article were defrayed in part by the payment of publication fees. Therefore, and solely to indicate this fact, this article is hereby marked "advertisement" in accordance with 18 USC section 1734.

Note

Supplementary data for this article are available at Cancer Research Online (http://cancerres.aacrjournals.org/).

Received November 22, 2021; revised June 15, 2022; accepted October 4, 2022; published first October 7, 2022.

References

1. Rauh-Hain JA, Gonzalez R, Bregar AJ, Clemmer J, Hernandez-Blanquisett A, Clark RM, et al. Patterns of care, predictors and outcomes of chemotherapy for ovarian carcinosarcoma: a national cancer database analysis. Gynecol Oncol 2016;142:38–43.
2. Mano MS, Rosa DD, Azambuja E, Ismael G, Braga S, D'Hondt V, et al. Current management of ovarian carcinosarcoma. Int J Gynecol Cancer 2007;17:316–24.
3. Rauh-Hain JA, Birrer M, Del Carmen MG. Carcinosarcoma of the ovary, fallopian tube, and peritoneum: prognostic factors and treatment modalities. Gynecol Oncol 2016;142:248–54.
4. Abeln EC, Smit VT, Wessels JW, de Leeuw WJ, Cornelisse CJ, Fleuren GJ. Molecular genetic evidence for the conversion hypothesis of the origin of malignant mixed mullerian tumours. J Pathol 1997;183:424–31.
5. Growdon WB, Roussel BN, Scialabba VL, Foster R, Dias-Santagata D, Iafrate AJ, et al. Tissue-specific signatures of activating PIK3CA and RAS mutations in carcinosarcomas of gynecologic origin. Gynecol Oncol 2011;121:212–7.
6. Jin Z, Ogata S, Tamura G, Katayama Y, Fukase M, Yajima M, et al. Carcinosarcomas (malignant mullerian mixed tumors) of the uterus and ovary: a genetic study with special reference to histogenesis. Int J Gynecol Pathol 2003;22:368–73.
7. Kounelis S, Jones MW, Papadaki H, Bakker A, Swalsky P, Finkelstein SD. Carcinosarcomas (malignant mixed mullerian tumors) of the female genital tract: comparative molecular analysis of epithelial and mesenchymal components. Hum Pathol 1998;29:82–7.
8. Gotoh O, Sugiyama Y, Takazawa Y, Kato K, Tanaka N, Omatsu K, et al. Clinically relevant molecular subtypes and genomic alteration-independent differentiation in gynecologic carcinosarcoma. Nat Commun 2019;10:4965.
9. Zhao S, Bellone S, Lopez S, Thakral D, Schwab C, English DP, et al. Mutational landscape of uterine and ovarian carcinosarcomas implicates histone genes in epithelial-mesenchymal transition. Proc Natl Acad Sci U S A 2016;113:12238–43.
10. del Carmen MG, Birrer M, Schorge JO. Carcinosarcoma of the ovary: a review of the literature. Gynecol Oncol 2012;125:271–7.
11. Barker HE, Scott CL. Genomics of gynaecological carcinosarcomas and future treatment options. Semin Cancer Biol 2020;61:110–20.
12. Fujii H, Yoshida M, Gong ZX, Matsumoto T, Hamano Y, Fukunaga M, et al. Frequent genetic heterogeneity in the clonal evolution of gynecological carcinosarcoma and its influence on phenotypic diversity. Cancer Res 2000;60:114–20.
13. Jones S, Stransky N, McCord CL, Cerami E, Lagowski J, Kelly D, et al. Genomic analyses of gynaecologic carcinosarcomas reveal frequent mutations in chromatin remodelling genes. Nat Commun 2014;5:5006.
14. Morishita A, Zaidi MR, Mitoro A, Sankarasharma D, Szabolcs M, Okada Y, et al. HMGA2 is a driver of tumor metastasis. Cancer Res 2013;73:4289–99.
15. Gattas GJ, Quade BJ, Nowak RA, Morton CC. HMGIC expression in human adult and fetal tissues and in uterine leiomyomata. Genes Chromosomes Cancer 1999;25:316–22.
16. Rogalla P, Drechsler K, Frey G, Hennig Y, Helmke B, Bonk U, et al. HMGI-C expression patterns in human tissues. Implications for the genesis of frequent mesenchymal tumors. Am J Pathol 1996;149:775–9.
17. Chang KP, Lin SJ, Liu SC, Yi JS, Chien KY, Chi LM, et al. Low-molecular-mass secretome profiling identifies HMGA2 and MIF as prognostic biomarkers for oral cavity squamous cell carcinoma. Sci Rep 2015;5:11689.
18. Piscuoglio S, Zlobec I, Pallante P, Sepe R, Esposito F, Zimmermann A, et al. HMGA1 and HMGA2 protein expression correlates with advanced tumour grade and lymph node metastasis in pancreatic adenocarcinoma. Histopathology 2012;60:397–404.
19. Saada-Bouzid E, Burel-Vandenbos F, Ranchere-Vince D, Birtwisle-Peyrottes I, Chetaille B, Bouvier C, et al. Prognostic value of HMGA2, CDK4, and JUN amplification in well-differentiated and dedifferentiated liposarcomas. Mod Pathol 2015;28:1404–14.
20. Sun M, Gomes S, Chen P, Frankenberger CA, Sankarasharma D, Chung CH, et al. RKIP and HMGA2 regulate breast tumor survival and metastasis through lysyl oxidase and syndecan-2. Oncogene 2014;33:3528–37.
21. Wang X, Liu X, Li AY, Chen L, Lai L, Lin HH, et al. Overexpression of HMGA2 promotes metastasis and impacts survival of colorectal cancers. Clin Cancer Res 2011;17:2570–80.
22. Park SM, Shell S, Radjabi AR, Schickel R, Feig C, Boyerinas B, et al. Let-7 prevents early cancer progression by suppressing expression of the embryonic gene HMGA2. Cell Cycle 2007;6:2585–90.
23. Helland A, Anglesio MS, George J, Cowin PA, Johnstone CN, House CM, et al. Deregulation of MYCN, LIN28B, and LET7 in a molecular subtype of aggressive high-grade serous ovarian cancers. PLoS ONE 2011;6:e18064.
24. Wang T, Wang G, Hao D, Liu X, Wang D, Ning N, et al. Aberrant regulation of the LIN28A/LIN28B and let-7 loop in human malignant tumors and its effects on the hallmarks of cancer. Mol Cancer 2015;14:125.
25. Tothill RW, Tinker AV, George J, Brown R, Fox SB, Lade S, et al. Novel molecular subtypes of serous and endometrioid ovarian cancer linked to clinical outcome. Clin Cancer Res 2008;14:5198–208.
26. Mahajan A, Liu Z, Gellert L, Zou X, Yang G, Lee P, et al. HMGA2: a biomarker significantly overexpressed in high-grade ovarian serous carcinoma. Mod Pathol 2010;23:673–81.
27. Funahashi Y, Okamoto K, Adachi Y, Semba T, Uesugi M, Ozawa Y, et al. Eribulin mesylate reduces tumor microenvironment abnormality by vascular remodeling in preclinical human breast cancer models. Cancer Sci 2014;105:1334–42.
28. Kashiwagi S, Asano Y, Goto W, Takada K, Takahashi K, Noda S, et al. Use of Tumor-infiltrating lymphocytes (TILs) to predict the treatment response to eribulin chemotherapy in breast cancer. PLoS ONE 2017;12:e0170634.
29. Yoshida T, Ozawa Y, Kimura T, Sato Y, Kuznetsov G, Xu S, et al. Eribulin mesilate suppresses experimental metastasis of breast cancer cells by reversing phenotype from epithelial–mesenchymal transition (EMT) to mesenchymal–epithelial transition (MET) states. Br J Cancer 2014;110:1497–505.
30. Cortes J, O'Shaughnessy J, Loesch D, Blum JL, Vahdat LT, Petrakova K, et al. Eribulin monotherapy versus treatment of physician's choice in patients with metastatic breast cancer (EMBRACE): a phase 3 open-label randomised study. Lancet 2011;377:914–23.
31. Katakami N, Felip E, Spigel DR, Kim JH, Olivo M, Guo M, et al. A randomized, open-label, multicenter, phase 3 study to compare the efficacy and safety of eribulin to treatment of physician's choice in patients with advanced non–small cell lung cancer. Ann Oncol 2017;28:2241–7.
32. Kaufman PA, Awada A, Twelves C, Yelle L, Perez EA, Velikova G, et al. Phase III open-label randomized study of eribulin mesylate versus capecitabine in patients with locally advanced or metastatic breast cancer previously treated with an anthracycline and a taxane. J Clin Oncol 2015;33:594–601.
33. Schoffski P, Chawla S, Maki RG, Italiano A, Gelderblom H, Choy E, et al. Eribulin versus dacarbazine in previously treated patients with advanced liposarcoma or leiomyosarcoma: a randomised, open-label, multicentre, phase 3 trial. Lancet 2016;387:1629–37.

34. Wakefield MJ. Xenomapper: mapping reads in a mixed species context. J Open Source Software 2016:1;18.
35. Harrison PF, Pattison AD, Powell DR, Beilharz TH. Topconfects: a package for confident effect sizes in differential expression analysis provides a more biologically useful ranked gene list. Genome Biol 2019;20:67.
36. Wakefield MJ. Survival volume: interactive volume threshold survival graphs. J Open Source Software 2016;1:111.
37. Barker HE, Chang J, Cox TR, Lang G, Bird D, Nicolau M, et al. LOXL2-mediated matrix remodeling in metastasis and mammary gland involution. Cancer Res 2011;71:1561–72.
38. Sreenan JJ, Hart WR. Carcinosarcomas of the female genital tract. A pathologic study of 29 metastatic tumors: further evidence for the dominant role of the epithelial component and the conversion theory of histogenesis. Am J Surg Pathol 1995;19:666–74.
39. Chiyoda T, Tsuda H, Tanaka H, Kataoka F, Nomura H, Nishimura S, et al. Expression profiles of carcinosarcoma of the uterine corpus-are these similar to carcinoma or sarcoma? Genes Chromosomes Cancer 2012;51:229–39.
40. Topp MD, Hartley L, Cook M, Heong V, Boehm E, McShane L, et al. Molecular correlates of platinum response in human high-grade serous ovarian cancer patient-derived xenografts. Mol Oncol 2014;8:656–68.
41. Barker HE, Patel R, McLaughlin M, Schick U, Zaidi S, Nutting CM, et al. CHK1 inhibition radiosensitizes head and neck cancers to paclitaxel-based chemoradiotherapy. Mol Cancer Ther 2016;15:2042–54.
42. Brackmann M, Stasenko M, Uppal S, Erba J, Reynolds RK, McLean K. Comparison of first-line chemotherapy regimens for ovarian carcinosarcoma: a single institution case series and review of the literature. BMC Cancer 2018;18:172.
43. Balzeau J, Menezes MR, Cao S, Hagan JP. The LIN28/let-7 pathway in cancer. Front Genet 2017;8:31.
44. Glaser G, Weroha SJ, Becker MA, Hou X, Enderica-Gonzalez S, Harrington SC, et al. Conventional chemotherapy and oncogenic pathway targeting in ovarian carcinosarcoma using a patient-derived tumorgraft. PLoS ONE 2015;10:e0126867.
45. Becker S, Kiecke C, Schafer E, Sinzig U, Deuper L, Trigo-Mourino P, et al. Destruction of a microtubule-bound MYC reservoir during mitosis contributes to vincristine's anticancer activity. Mol Cancer Res 2020;18:859–72.
46. Alexandrova N, Niklinski J, Bliskovsky V, Otterson GA, Blake M, Kaye FJ, et al. The N-terminal domain of c-Myc associates with alpha-tubulin and microtubules *in vivo* and *in vitro*. Mol Cell Biol 1995;15:5188–95.
47. Tanni KA, Truong CB, Johnson BS, Qian J. Comparative effectiveness and safety of eribulin in advanced or metastatic breast cancer: a systematic review and meta-analysis. Crit Rev Oncol Hematol 2021;163:103375.
48. Liu M, Xia Y, Ding J, Ye B, Zhao E, Choi JH, et al. Transcriptional profiling reveals a common metabolic program in high-risk human neuroblastoma and mouse neuroblastoma sphere-forming cells. Cell Rep 2016;17:609–23.
49. Zhao W, Prijic S, Urban BC, Tisza MJ, Zuo Y, Li L, et al. Candidate antimetastasis drugs suppress the metastatic capacity of breast cancer cells by reducing membrane fluidity. Cancer Res 2016;76:2037–49.
50. Tabas I. Consequences of cellular cholesterol accumulation: basic concepts and physiological implications. J Clin Invest 2002;110:905–11.
51. Abdulla N, Vincent CT, Kaur M. Mechanistic insights delineating the role of cholesterol in epithelial–mesenchymal transition and drug resistance in cancer. Front Cell Dev Biol 2021;9:728325.
52. Huang B, Song BL, Xu C. Cholesterol metabolism in cancer: mechanisms and therapeutic opportunities. Nat Metab 2020;2:132–41.
53. Zhang M, Yan Z, Wang J, Yao X. Toll-like receptors 7 and 8 expression correlates with the expression of immune biomarkers and positively predicts the clinical outcome of patients with melanoma. Onco Targets Ther 2017;10:4339–46.
54. Gatti G, Betts C, Rocha D, Nicola M, Grupe V, Ditada C, et al. High IRF8 expression correlates with CD8 T-cell infiltration and is a predictive biomarker of therapy response in ER-negative breast cancer. Breast Cancer Res 2021;23:40.
55. Raieli S, Di Renzo D, Lampis S, Amadesi C, Montemurro L, Pession A, et al. MYCN drives a tumor immunosuppressive environment which impacts survival in neuroblastoma. Front Oncol 2021;11:625207.
56. Goto W, Kashiwagi S, Asano Y, Takada K, Morisaki T, Fujita H, et al. Eribulin promotes antitumor immune responses in patients with locally advanced or metastatic breast cancer. Anticancer Res 2018;38:2929–38.